Delft Cluster

Title:	**Stability of Coarse Granular Structures** **investigation on micro-scale**		
Author:	ir B. Hofland	Institute:	Delft University of Technology
			December 2002

Number of pages	:	73 (including appendices)
Keywords (3-5)	:	Granular material, critical shear stress, bed protection, turbulence
DC-Publication-number	:	03.02.04-02
Institute Publication-number (optional)	:	-
Report Type	:	☐ Intermediary report or study
	:	☒ Final project report
DUP-publication Type	:	☒ DUP Standard
		☐ DUP-Science

Other Research project sponsor(s):

Ministry of Transport, Public Works
and Water Management

Abstract

The aim of the project described in this report is to identify and investigate the physical mechanisms that lead to damage of the top layer of granular bed protections. In this process the turbulent force fluctuations are a key factor. The type of flow considered is stationary, non-equilibrium, low-mobility flow over hydraulically rough beds.

Flume experiments were done on the flow near, and the pressures on a cubical element in a granular bed consisting of one layer of angular stones. Two different force-generating mechanisms were considered; the quasi-steady mechanism and the turbulence-wall-pressures (TWPs) mechanism. The quasi-steady fluctuating forces are caused by the mechanism which also causes the mean forces. These forces are mainly dependent on the longitudinal velocity ($F \propto u^2$). The TWPs-induced forces arise from the pressure gradients that are inherent to a turbulent flow field. Three flow situations were investigated: the equilibrium uniform flow, the backward-facing step, and the beginning of a granular bed (roughness transition). It seemed that the quasi-steady mechanism was dominant in most cases: here low frequency fluctuations of the longitudinal velocity cause low frequency variations of the (drag) force. The maximal forces occur during periods with downward directed flow (Q_4-events). The TWPs-induced forces do have a significant influence on stones that are shielded by stones upstream of them. These are normally not the unstable stones, except for bed protections with a large range of stone sizes, where the unstable small stones are shielded. Ten step-heights behind a backward-facing step the TWPs had a large influence on the total variance of the forces. However, the maximum forces were still caused by the quasi-steady mechanism (appendices A and B).

A (numerical) discrete particle model was developed in order to estimate the positions of the most exposed particles, which are expected to move first. Using this model, the process of sequentially dropping equally sized spheres was simulated. Next the upper particles were removed from these simulated beds, simulating the effect of entrainment. This resulted in a flatter bed-topography that is more stable than when it is just deposited. It was concluded that for this case the statistics of the micro bed-topography are not dependent on the way that the particles are deposited (appendix C).

The set-up for the new experimental facilities and the measurement technique particle image velocimetry (with which we can measure entire flow fields instantaneously) are described. With these whole-field measurements the coherent flow structures responsible for the extreme forces can be measured (appendices D and E).

PROJECT NAME:	**A: Bed Protections**	PROJECT CODE:	**03.02.04**
BASEPROJECT NAME:	**Behaviour of coarse-grained structures**	BASEPROJECT CODE:	**03.02**
THEME NAME:	**Coast and River**	THEME CODE:	**03**

Executive Summary

This report describes the progress of a PhD project on bed protections during the period that it was funded by Delft Cluster. Bed protections near hydraulic structures are often composed of several filter layers consisting of loose granular material (riprap). In order to assess the chance on damage to these filter layers, the stability of the rocks in the top layer has to be known. Until now only empirical relations are known for the determination of the stability of these granular filters. Especially for non-uniform flows these relations have limited validity. The goal of the present research is to formulate a model, based on physical processes, that describes the stability of loose granular materials (riprap) under non-uniform flows. For this a fundamental understanding of the physical processes causing damage is needed. Especially the influence of the turbulence on the extreme forces on the stones is of importance.

The influence of the turbulence structure on the fluctuating forces on a single stone has been investigated experimentally. Flume experiments were done on the flow near, and the pressures on a cubical element in a granular bed, consisting of one layer of angular stones. Velocity was measured by laser-doppler velocimetry, and pressures were measured by piezometric, miniature pressure transducers.

Two different force-generating mechanisms were considered; the quasi-steady mechanism and the turbulence-wall-pressures (TWPs) mechanism. The quasi-steady fluctuating forces are caused by the mechanism which also causes the mean forces. These forces are mainly dependent on the longitudinal velocity ($F \propto u^2$). The TWPs-induced forces arise from the pressure gradients that are inherent to a turbulent flow field. Three flow situations were investigated: the equilibrium uniform flow, the backward-facing step, and the beginning of a granular bed (roughness transition). It seemed that the quasi-steady mechanism was dominant in most cases: here low frequency fluctuations of the longitudinal velocity cause low frequency variations of the (drag) force. The maximal forces occur during periods with downward directed flow (Q_4-events). The TWPs-induced forces do have a significant influence on stones that are shielded by stones upstream of them. These are normally not the unstable stones, except for bed protections with a large range of stone sizes, where the unstable small stones are shielded. Ten step-heights behind a backward-facing step the TWPs had a large influence on the total variance of the forces. However, the maximum forces were still caused by the quasi-steady mechanism.

A (numerical) discrete particle model was developed in order to estimate the positions of the most exposed particles, which are expected to move first. Using this model, the process of sequentially dropping equally sized spheres was simulated. Next the upper particles were removed from these simulated beds, simulating the effect of entrainment. This resulted in a flatter bed-topography that is more stable than when it is just deposited. It was concluded that for this case the statistics of the micro bed-topography are not dependent on the way that the particles are deposited.

The project will continue after the Delft Cluster involvement. The set-up for the new experimental facilities and the measurement technique particle-image velocimetry (with which we can measure entire flow fields instantaneously) are described. The new facility will be used to measure the conditionally averaged flow field at the moment that a single particle is moved from the bed.

All of the above will ultimately lead to a better description of the influence of turbulence on stone stability which could lead to the development of (numerical) models for predicting damage.

PROJECT NAME:	**A: Bed Protections**	PROJECT CODE:	**03.02.04**
BASEPROJECT NAME:	**Behaviour of coarse-grained structures**	BASEPROJECT CODE:	**03.02**
THEME NAME:	**Coast and River**	THEME CODE:	**03**

Table of contents

-A. Draft paper for scientific journal

-B. Paper to be published in proceedings Monte Veritá symposium

-C. Discussion for Journal of Hydraulic Engineering regarding DPM

-D. Description of new experimental set-up

-E. Laser safety report

-F. General Appendix: Delft Cluster Research Programme Information

1 Introduction

This is the final report for the Delft Cluster project: 'Behaviour of Coarse Granular Structures, part A', which is part of basic project 2: 'Hydraulic and Geotechnical Engineering', under the theme 'Coast and River'.

In this report the results of the project are explained and compared to the original project description. The entire project has started at 1-4-2000 and is planned to take place until 1-4-2004. Delft Cluster is cosponsor of the project until 31-12-2002. The other sponsor is the Road and Hydraulic Engineering Division of the Ministry of Transport, Public Works and Water

Management (DWW). The research is mainly executed by Ph.D. candidate ir. B. Hofland, guided at Delft University of Technology by: prof.dr.ir. J.A. Battjes, prof.ir. K. d'Angremond, drs. R. Booij, dr.ir. H.L. Fontijn and ir. H.J. Verhagen. The persons that guided the project in the biannual Delft Cluster meetings are mentioned in Appendix F.

The aim of the project is to gain insight into the physical processes that determine damage to bed protections. The main focus is on the determination of the influence of turbulence on the initial movement of stones in the top layer of a granular filter under stationary, non-equilibrium flows.

The following chapters in the report describe the progress as compared to the original project description and the planning for the next period. The substantive results are mainly presented in the appendices, which are a collection of the reports and papers that were the result of the project. Appendix A is the outcome of the final analysis of the first series of experiments. It regards the influence of near-bed turbulence on stone stability. It is too long for a single paper in a peer-reviewed scientific journal. Therefore it will either be decreased in length, or split into two separate papers. Appendix B is the paper that will be published in the proceedings of a conference that was attended in Monte Veritá, Switserland. It comprises part of the content that was used in appendix A. Appendix C is a discussion which describes the numerical model that was made for determining the positions of stones in a randomly deposited granular bed. Appendices D and E describe the new experimental facility and apparatus that will be used during continuation of the research.

2   Realisation

The original project description mentions 'making experimental set-up', 'finding pressure sensors' en 'literature survey' as the aims of the first year. All this has been accomplished. Suitable pressure sensors were found relatively quickly, and a filtering technique for cancelling spurious environmental pressures was developed. An experimental set-up was made that was used for the first set of trial experiments of pressures on a flat bed and on a surface-mounted cube. This set-up was not the final set-up that is going to be used. Nevertheless, it could be used for the measurements in the second year, which were intended to regard a simplified configuration. The simplified characteristics were the facts that the bed consisted of one layer of stone and that the shape of the instrumented stone was cubical. Still the configuration resembled a granular bed protection quite well. Laser Doppler Velocimetry was used together with the pressure sensors (three pressure sensors were installed in the cube), so that the relation between pressures and velocities could be investigated directly. Besides experiments on a uniform flow, experiments were done on flows with an altered turbulence structure, which are mentioned as a key part of the research in the project plan. The analysis of these experiments is completed.

The set-up for a new series of experiments is now complete. These experiments have not been executed yet. It took some time to acquire, test and install the new measurement set-up of the PIV system (mentioned in the project plan). The measurements will be undertaken during the continuation of the project.

As an additional project a numerical model (discrete particle model, or DPM) was developed during the second year, which was used to estimate the distribution of the positions of the top particles in a bed. Numerical flow calculations have not been executed. However, calculations on a bed-mounted cube on a smooth wall are available at the Aero- & Hydrodynamics Section at the faculty of WBMT and these might be used later during the modelling phase.

3   Answered and open questions

At the moment we have increased the understanding of the generation of the forces and pressures that act on a stone. A distinction has been made between several force-generating mechanisms, and about their contribution to the total force on a stone. Also non-uniform flows have been studied, and it could be seen how the length scales of the dominant turbulent eddies change, and what the contributions of the various mechanisms are. Therefore we are beginning to understand how a non-equilibrium flow can damage a bed protection. The discrete particle model gave some insight into the stone placement as well.

A 'Q_4-event' is an instantaneous flow direction with increased longitudinal velocity and downward vertical velocity. These events probably create most damage, as the maximum values of u' occur in this quadrant. But what does a 'Q_4-event' near the bed represent? Is it a random direction of the flow, or is a 'Q_4-event' linked to a certain 'coherent' flow structure, as has been proven for flow over smooth walls? If this is the case we want to know whether these coherent structures are similar. All this can hardly be answered without spatially distributed velocity measurements. Therefore the PIV-measurements were initiated.

At the moment, it is thought that the large-scale velocity fluctuations are most important for the stone stability. This would mean that if the large-scale turbulent motion could be resolved by Large Eddy Simulation (LES), the indicators that predict damage to bed protections could be obtained. Whether this is really the case, should be investigated by comparing LES results to measurements.

4   Continuation

The project will be continued after the formal Delft Cluster involvement has terminated. During the end of the third and beginning of the fourth year the second series of experiments –using the new PIV set-up which enables us to measure instantaneous flow fields– will be executed and analysed. The same three configurations will be examined as during the first series (uniform flow, beginning of bed

and backward-facing step). An M.Sc. student, R. de Ruiter, is going to execute the backward-facing step experiments. The attached paper on the first series of experiments will be compiled into an acceptable form for a scientific journal. With the results of the literature survey, and the two series of experiments we will try to formulate the important parameters that indicate stone stability, and how they change for different flow situations. If there is enough time some results of larger scale modelling by LES will be used. No separate roughness elements will be regarded, but it will be used to see whether the parameters needed for the prediction of damage to bed protections can be predicted by LES computations. This will indicate whether LES calculations could be used as a design tool for bed protections besides physical modelling. The Ph.D. thesis will be written as well in the fourth year.

5 Meetings

The following meetings with the 'Klankbordgroep' and 'Begeleidingsgroep' have been held during the entire project period:

- 05-12-2000: Kick-off-meeting with Begeleidingsgroep + Klankbordgroep.
- 08-05-2001: Meeting with Begeleidingsgroep.
- 13-12-2001: Meeting with Begeleidingsgroep + Klankbordgroep.
- 21-6-2002: Meeting with Begeleidingsgroep.
- Last meeting with Begeleidingsgroep + Klankbordgroep: 05-12-2002

6 Reports ('deliverables')

The following list of reports, articles, etc. which were written during the course of the project until now includes almost all 'deliverables' that were envisaged in the original project plan. A plan of approach was written, and eight quarterly progress reports were written. A literature survey was conducted [1], and several reports were written on the experimental results and techniques [2, 3, 5]. Also scientific output was produced [6, 7]. The draft article that is included in this report will also be used as the basis for one or two journal papers, and as a part of the final thesis. As no major numerical work has been undertaken (it was decided to undertake two series of experiments), there is no report about that, despite the fact that it was in the list of 'deliverables'.

1] HOFLAND, B. 2000. *Stability of stones in the top layer of a granular filter – literature survey*, Tech. Rept. 07-00, Environmental Fluid Mechanics Section, Delft University of Technology.

2] HOFLAND, B. 2001. *Pressure Sensors and Filtering Techniques for Stone Stability Assessment*, Tech. Rept. 04-01, Environmental Fluid Mechanics Section, Delft University of Technology.

3] HOFLAND, B. 2001. *Report on measurements*: *Pressure and velocity fluctuations and around a granular bed element*, Tech. Rept. 06-01, Environmental Fluid Mechanics Section, Delft University of Technology.

4] HOFLAND, B. 2002. *Conditional sampling of pressure and velocity measurements for investigation of the entrainment mechanism of coarse particles*, Technical note.

5] HOFLAND, B. 2002. *Veiligheidsrapport m.b.t. de metingen in de PIV-goot in het Laboratorium voor Vloeistofmechanica*, Tech. Rept. 05-02, Environmental Fluid Mechanics Section, Delft University of Technology.

6] HOFLAND, B. 2003. *Discussion on "Discrete Particle Modelling of Entrainment from Flat Uniformly Distributed Sediment Beds", by I. McEwan & J. Heald*, Journal of Hydraulic Engineering 129 (1).

7] HOFLAND, B., BOOIJ, R, AND FONTIJN, H.L.2003. *Entrainment of large particles from granular bed protections under low-mobility transport conditions.* Proceedings of "Sediment transport and Sedimentation", Monte Veritá, Switserland 2002

7 Appendices

- A. Draft paper for scientific journal

- B. Paper to be published in proceedings Monte Veritá symposium

- C. Discussion for Journal of Hydraulic Engineering regarding DPM

- D. Description of new experimental set-up

- E. Laser safety report

- F. General Appendix: Delft Cluster Research Programme Information

Appendix A. Draft paper for scientific journal

Near-bed turbulence and stone stability
theory and measurements
DRAFT

Bas Hofland

November, 2002

Contents

Abstract

To be made...

1 Introduction

1.1 Rationale

This paper treats the entrainment of particles from hydraulically rough beds under low-mobility flow conditions. Knowledge about this process is needed for the determination of the strength of bed protections near hydraulic structures like revetments and breakwaters (Pilarczyk, 2001) and for predictions of morphological developments in seas and rivers (Thorne *et al.*, 1989; Andrews & Smith, 1992). In this flow regime the turbulence fluctuations of flow and pressure are a key factor in the entrainment of bed particles. The forces on a bed particle scale with the shear stress under an equilibrium wall flow, so for this flow the shear stress can be used as an indicator for entrainment and transport (Shields, 1936) without knowing the exact force-generating mechanisms. However, as most flows encountered in the engineering practise are non-equilibrium, more detailed knowledge of the transport processes is needed. Entrainment, as the first step in the transport process, must therefore be studied in detail. Upscaling results from experiments in small flumes to prototype situations requires the detailed knowledge of the processes as well.

Numerous physical model tests have been undertaken on morphological bed changes and on damage to bed protections. Also, theoretical models have been made for the beginning of

movement, mostly based on analyses of the balance of force moments on a particle. Still these micro-models have hardly been compared to measurements on a micro level. The outcome is usually directly compared to integrated transport measurements, which have large errors, making it difficult to establish the quality of the models. Models determining the mean forces on particles have been compared to measurements, but the fluctuating forces, which are a key factor for the actual movement under low-mobility transport conditions, have hardly been compared. Of course it is difficult to undertake this, as there is an unlimited number of possible particle positions. This has resulted in the situation where the exact mechanisms that cause the entrainment of a particle from a rough bed are still unknown.

Under low-mobility transport conditions (with a shear stress under the so-called critical shear stress) transport of particles is difficult to determine. The random character of the turbulent flow and of the micro bed topography (on the scale of a particle the bed is far from flat) causes a high uncertainty in most measurements. The slope of transport curve as a function of shear stress is steep (Paintal, 1971), which makes that a small error in the determination of the shear stress (which is difficult to do with the required precision) gives a large error in the determination of the transport curve. When the physical mechanism which induces entrainment is known, it becomes feasible to describe the probability of entrainment by regarding the probability density function (PDF) of the positions of the most exposed stones (varying per stone) and of the forces on the stones (varying in time) as introduced by Grass (1970). For rough beds a stochastic approach is also pursued by Papanicolaou *et al.* (2002).

1.2 Problem description

The type of flow considered is flow over a hydraulically rough bed, so viscous forces are negligible. As we consider low-mobility transport, the flow is not disturbed by the occasionally moving particles. Therefore the pressures on a single element in a fixed bed need to be considered. When a particle moves, it will either be rotated over a downstream particle, or slide over it. It is highly unlikely that saltation will occur. The flow that we are examining can be described by the following characteristics:

- Rough bed (particle Reynolds number, $Re* > 500$, viscous forces negligible)

- Narrow size distribution ($d_{85}/d_{15} < 1.5$)

- Low mobility ($\tau/\rho\Delta gd \approx 0.03$–$0.05$ for uniform flow)

    - flat bed
    - bed load by sliding / rolling
    - flow as over fixed bed
    - one stone moves at a time

– micro bed topography is important

- Stationary flow

1.3 Mechanisms

Under low-mobility transport conditions a particle will only move when the fluctuating part of the force exceeds a certain value. Therefore we will concentrate on the generation of (extreme) pressures by (extreme) flow events in the turbulent flow over the bed. We will distinguish two force-generating mechanisms.

Under high Reynolds numbers, the mean values of the forces on a bed particle are caused by accelerations due to the streamline curvature of the flow passing the stone. These forces are often referred to as drag and lift. These forces are a function of the longitudinal flow ($F \propto u^2$), which is the mean flow direction near the bed. If the ambient longitudinal velocity fluctuates, this will therefore lead to fluctuating forces on a stone. These fluctuations will be referred to as quasi-steady forces.

In a turbulent flow, however, acceleration of water parcels and streamline curvature are always present, also away from the boundaries. These accelerations are directly linked to pressure gradients via Newton's third law. Therefore, near a wall the turbulence creates fluctuating pressures on the bed, even when it is smooth. These turbulence wall pressure fluctuations (TWPs), when integrated over a bed particle, will result in nett forces on the stone and therefore contribute to the fluctuating forces on a stone. Whether the TWPs can give a significant contribution to the extreme forces on the bed-particles, will be examined in this paper.

1.4 Size shape and position of particles

In this paper the terms drag and lift (force) will often be used. They are defined as the horizontal and vertical force components. For the mean forces this is equal to the force components in line with, and normal to the flow direction respectively, as the mean flow over the bed is horizontal. However, for the instantaneous force, which can have a vertical component, the drag force is not in-line with the instantaneous flow anymore.

In the past it was often assumed that either the lift component is responsible for dislodging particles from the bed (Einstein & El-Samni, 1949, for example) or that drag is fully responsible (White, 1940; Egiazaroff, 1965, for example). In later models (Wiberg & Smith, 1987) both force components are included, with the drag force indicated as the largest force component, although some recent articles still use the concept that only lift is important (Cheng & Chiew, 1998, for example). Which force component is responsible is of course dependent on the position of the particle, which can be described to a large extent by its relative protrusion, Π/d (Π is protrusion, and d is diameter of the stone). If $\Pi/d \approx 1$ then the particle is nearly completely exposed and a large drag force will be present. Further, the

angle of repose, ϕ, is then in general such that a drag force gives a large moment a round the point of rotation, making this component very effective. If $\Pi/d \approx 0$ then obviously only lift force can efficiently create large moments. Measurements of Fenton & Abbot (1977) showed that the critical shear stress decreases in an exponential fashion when increasing the relative protrusion. Both the resisting moment ($\approx Gd \sin\phi$) decreases, and the attacking (drag) force increases. However, they did not measure what the specific contribution of the drag and lift force were for different protrusions.

1.5 Aim

The general aim of this study is to increase the knowledge on the displacement mechanisms of coarse particles under low-mobility transport conditions. A few specific aims can be derived from this. A first aim is to look at the influence of the protrusion of the particle on the two force components separately. The second aim is to investigate whether the TWPs (see 1.3) have a significant influence on the forces on the bed particles, relative to the quasi-steady contribution. Thirdly, next to studying the equilibrium open-channel boundary-layer flow, we want to investigate how the fluctuating forces on a bed particle change the flow configuration is altered. Although the resisting force of the particles is of importance, this paper mainly focusses on the possible force-generating mechanisms. In later analyses the distributions of particle characteristics like angle of repose, imbrication, shielding, shape, etc. will have to be taken into account.

1.6 Approach

In this paper we first theoretically examine the possible entrainment mechanisms. Both for the quasi-steady mechanism and the newly proposed force generating mechanism (by TWPs) it is derived which characteristics in the measurements indicate their presence and significance. Then measurements of fluctuating pressures on and velocities near a bed fixed element are presented. After this, the measurement results are discussed in the light of the theory. First this is done for case of uniform ambient flow. A detailed analysis is made of the origin of extreme pressures, as these are expected to dislodge the particles. Two major kinds of data analysis are used. The first is a quadrant analysis of the pressures, following Nelson *et al.* (1995). The second is the determination of the conditionally averaged pressures during extreme values of band-pass filtered velocity signals. Two different beds with randomly placed stones are used to see whether the protrusion has a universal influence. Finally, two non-equilibrium flow configurations are considered. The bed structure for these configurations is equal to one of those used for the uniform flow cases so that the only parameter varied is the turbulence structure. In order not to make the configurations too complicated, only two-dimensional flows are considered. These are approximately present in many prototype situations such as the flow at the beginning of a granular bed (roughness transition), and

the flow behind a backward-facing step. Measurements were taken at only one longitudinal position for all configurations.

2 Previous research on entrainment mechanisms

Kalinske (1947) regarded only drag as the force dislodging the particles from the bed. He gave two possible sources for fluctuating forces on a particle. The first was the unsteady separation of the flow from the particle, causing the drag force to fluctuate. The second was the larger scale turbulence fluctuations from the main stream.

Einstein & El-Samni (1949) also recognised that turbulence induced fluctuations are important for the entrainment of particles from granular beds. They measured the fluctuating pressures on a sphere and postulated that lift was the most important force component for entrainment. This is true for their configuration of densely packed spheres ($\Pi/d = 0$), but probably not for particles on a natural bed.

Sutherland (1967) visualised the flow during the entrainment of sand from a plane bed and from a dune bed by dye injection. Re_* was rather low, with values ranging from 0.25 to 2, therefore the thickness of the viscous sublayer was larger than the grain diameter, making this configuration different than the one of the present investigation.

For the plane bed case, it was observed that the entrainment of particles was correlated to ejections of parts of unstable low speed streaks near the bed (these flow events are nowadays known to be part of the so-called bursting cycle, the main near-bed instability which causes the momentum transfer to the main flow). Always several particles moved at the same time, indicating that the size of the eddy responsible for movement was larger than the grain size. In the case with the dune bed, which is comparable to a series of backward-facing steps, particles were displaced first at the reattachment point, although flow velocities are low at that position. They were moving in a random, jerky manner. Sometimes small "craters" were visible, indicating the impingement of eddies with a high vertical momentum. These eddies were modelled by a pulsating jet above a sand bed, which created vortex rings that impinged on the bed. It could be seen that particles were first made to move horizontally away from the centre of the vortex ring due to the high horizontal flow velocity. At the outer edge of the vortex, the flow has an upward vertical component, and only here the particles were lifted from the bed. Hydrodynamic lift, pressure gradients in the eddy, vertical forces due to contacts with other particles, and upward flow through the porous bed were attributed a possible minor role in the entrainment process.

Grass (1970) used hydrogen bubble visualisation in order to measure the instantaneous flow profile near a sand bed. Grain Reynolds numbers, Re_*, were again very small at 0.2 to 2. Because the thickness of the viscous sublayer was larger than the grain diameter, the instantaneous shear velocity could be determined by the slope of the (linear) velocity profile in the viscous sublayer ($u_* = \sqrt{\nu \frac{du}{dy}}$). Transport occurred during events with a large shear

stress. Grass introduced the concept that both the shear stress and the critical shear stress are stochastically distributed, and that entrainment commences if the (instantaneous) shear stress is greater than the (local) critical shear stress. The subsequent probabilistic treatment of the determination of the critical shear stress was not entirely correct (Hofland, 2000).

Nelson *et al.* (1995) presented some concepts that are also used in this work. Experiments were done on the entrainment of coarse sand with $Re_* \approx 22.5$. This means that some grains were protruding through the viscous sublayer, making this research more similar to our work (where $Re_* \approx 3000$) than the other research mentioned. Flow velocity and transport were measured at various positions behind a backward-facing step (step height = 0.2 water depth). Quite some transport occurred, as the dimensionless shear stress, ψ (far behind the step), was twice the critical shear stress, ψ_c (≈ 0.055). Measurements were made of the vertical and streamwise velocity by LDV and the sediment transport was determined from high speed film recordings of the bed. The flow attached about 6 step heights downstream from the step. The shear velocity had a broad maximum 15-30 step heights from the step, and was slightly lower downstream of that. The maximum $\sqrt{\overline{u'^2}}$ was measured at 10 step heights from the step, but the highest transport was measured at 20 step heights from the step. Velocity and transport were correlated in order to find out which turbulence events cause transport. Especially the longitudinal velocity fluctuations (u') were correlated to transport of grains. Instantaneous values of $-u'v'$ and $-v'$ were both positively correlated to the transport as well, only less clearly. It was expected that the velocity fluctuations with frequencies higher than those of the fluctuations introduced by the mixing layer downstream of the step would not be correlated to sediment transport. These high frequency fluctuations would therefore decrease the correlation between velocity and transport. Therefore the velocity signal was low-pass filtered with various cut-off frequencies, whereby it was initially expected that the correlation between velocity and transport would increase with decreasing cut-off frequencies until cut-off frequencies corresponding to the fluctuations induced by the large scale turbulence behind the step (< 2 Hz) were reached. However, removing fluctuations with frequencies higher than 10 Hz already yielded the highest correlation. This is surprising, as the frequencies of the high magnitude velocity fluctuations caused by the step were lower. This led to the conclusion that both low frequency fluctuations (0.1 to 2 Hz) and high frequency fluctuations (2 to 10 Hz and even higher) contributed to the transport. Plotting the average transport rate for all (u',v') combinations as a function of u' and v' showed that transport increased with increasing u'. A transfer function deduced from all measurements, which showed the average transport rate for all (u',v') combinations, gave peaks in both Q_1 and Q_4 quadrants (for definitions see figure 11). The transfer function did not perform well in predicting the actual instantaneous transport. The reason given in the article is that low frequency u' gives more transport than high frequency u', as the amount of transport increases nonlinearly (exponent greater than one) with an increase of the time scale of the velocity fluctuation.

Gyr & Schmid (1997) studied the incipient motion from a smooth sand bed by the hairpin

eddies of the well known bursting cycle. Based on the pattern of the displaced sand they conclude: "When a sweep consisting of a patch of spanwise limited fast outer fluid, hits the bed, the fast fluid from the outer flow regions is decelerated and produces very concentrated vorticity at its edges. These vortex cores have a high under-pressure which is the motor for the sediment transport. The resulting transport is directed mainly sideways from the impact area and produces a sand stripe on each side of the sweep." This could be seen as a direct influence of the TWPs on entrainment. The viscosity-dominated bursting cycle does not exist over rough walls, so this idea cannot be applied to this flow regime. Based on a comparison of the sizes of the coherent structures and the grain sizes they conclude that always several grains will move at once, and that: "The study of incipient motion of single grains (...) only makes sense for fairly large grains".

Several investigations have been done on the forces on single elements. An overview until 1993 is given in Xingkui & Fontijn (1993). Not many simultaneous measurements of the instantaneous forces or pressures on and the velocity near a particle have been made, except for the measurements by Radecke & Schulz-DuBois (1988), who simultaneously measured the lift force on a sphere near a smooth wall and the velocity (in vertical and streamwise direction) just upstream of it. This configuration is not a realistic model for a natural stone, but the transfer functions between both velocity fluctuation components and the lift force, do give some information about force generating mechanisms. A second investigation is by Xingkui & Fontijn (1993) who measured the two force components on a naturally-shaped bed element and two velocity components simultaneously at several positions behind a backward-facing step.

3   Quasi-steady forces

As indicated in section 1.3 we will consider two force-fluctuation generating mechanisms. The first one will be referred to as the quasi-steady force, as it is an extension of the mechanism causing the mean forces. It will be discussed rather briefly in this section, in spite of it being the most significant force.

The mean drag and lift force on the particles are given by the well known law $F_{d/l} = \frac{1}{2}C_{d/l}A\rho u^2$ (for the drag and lift force the coefficient, C, and area, A, are different). If the ambient flow velocity is rather uniform and does not change too rapidly, the fluctuating drag force will become proportional to:

$$F'_d \propto \tfrac{1}{2}\left(\rho u(t)^2\right)' \approx \rho U u' \ \left(+\rho u'^2\right) \tag{1}$$

In which u is split in a mean part U and a fluctuating part u'. If the assumption $u' << U$ is made, the second term of the right-hand-side can be neglected. However, for the extreme values of u' close to the bed, $u' << U$ is not true anymore, as the fluctuation can be of the same magnitude as the mean value, see for instance the velocity distribution in figure 11. Still

$u' < U$ holds for configuration with uniform ambient flow, so the first term will be dominant. The flow velocity near the bed has a large vertical gradient. This makes the choice of the y coordinate ambiguous. Only for a very protruding particle it was shown that the centre velocity and C_{d} for a sphere in free fall can be used (Coleman, 1972). If all particles have the same position, then the drag force is simply equal to the particles' representative area (total area divided by number of particles, is $\frac{1}{2}\sqrt{3}d^2$ for densely packed spheres, for instance) times the shear stress (Watters & Rao, 1971). It can be expected that this drag force will be caused mainly by relatively slow variations in the flow velocity. Power spectra of u' usually tend to have negative slopes for the higher frequencies, so the largest magnitudes of this force are expected at the lower frequencies (magnitude of mean velocity divided by the water depth).

For the quasi-steady fluctuating lift the following relation will hold:

$$F_{\mathrm{l}}' \propto aUu' + bUv' \tag{2}$$

The first term on the right hand side is caused by the Bernoulli-effect, it being the linear expansion of $F_{\mathrm{l}} \propto u^2$ ($u' << U$). Furthermore, the instantaneous flow direction does not have to be horizontal like the mean flow. Therefore, the instantaneous force in line with the velocity (caused by the stagnation pressure) can have a vertical component ($F_{\mathrm{l}} = \frac{1}{2}C_{\mathrm{d/l}}A\rho\|\vec{u}\|v$). A linear expansion of this leads to the second term in eq. (2). Radecke & Schulz-DuBois (1988) used eq. (2) to determine the gain function from the velocity spectrum to the force spectrum. Using these gain functions they could predict 20–70% of the power spectrum of the forces on a sphere on a flat plate. The spectrum for the lowest frequencies was almost exactly predicted from the measured gain functions. Most of the variance originated from the u fluctuations [first term on the right hand side of eq. (2)]. The second term caused a small part of the variance at a frequency band, related to the Strouhal number.

To summarise the above, we expect that –if the quasi-steady mechanism is significant– low frequency, positive, extreme values of u' will correspond to increased values of the drag and lift force components. For the lift, a positive v' might also contribute to the high frequency lift force.

If the plane of possible (u',v')-combinations is divided in four quadrants, it can be seen that the velocity vector for a shear flow is mainly present in quadrants 2 and 4 (Q_2 and Q_4). The names for the quadrants in the (u',v') plane were given according to the definition linked to certain smooth-wall coherent structures in the bursting cycle: sweeps (Q_4) and ejections (Q_2). These names are often used for flows over rough beds as well, or for non-equilibrium flows (Raupach, 1981; Nelson *et al.*, 1995, for instance). As the turbulence structures that cause a certain direction of the velocity vector can be different here, we will simply refer to a velocity vector in quadrant 2 as a Q_2-event, for example, instead of ejection. The magnitude and frequency of occurrence of Q_2- and Q_4-events changes over the height of the flow (Raupach, 1981). During Q_4-events, the longitudinal flow velocity is highest, and most transport is seen to occur during these events (Nelson *et al.*, 1995).
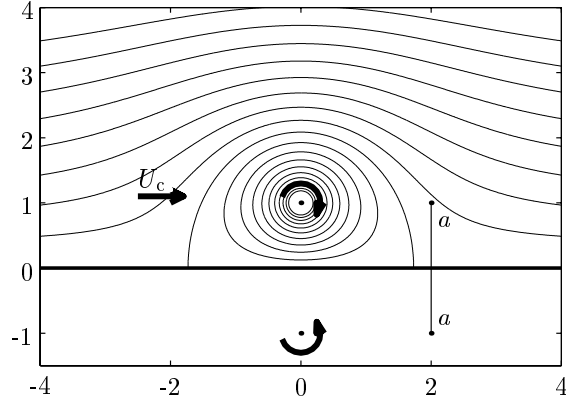
9

Figure 1: Streamlines around a point vortex near wall, in a frame of reference moving with the vortex.

4 Turbulence wall pressures (TWPs)

4.1 Model-vortex

In order to illustrate what the direct influence of an eddy on stone stability can be, we regard a simplified model-vortex, as described by Doligalski *et al.* (1994). We can infer a few characteristics of the pressure field that is induced by a vortex from this model. With this we can make it plausible that the pressures caused by the vortex have an effect on the fluctuating forces on the stone.

A vortex is modelled as a point containing vorticity, surrounded by potential flow. We will adopt the following definitions. U_0 is the free stream velocity in infinity, κ is the strength of the vortex, a is the height of the vortex above the wall, and α is the fractional convection rate of the vortex, $\frac{V_c}{U_0} = 1 - \frac{\kappa}{2aU_0}$. The stream function, ψ, that can be obtained for the flow field of the model vortex above a wall, in a frame of reference moving with the vortex, illustrated in figure 1. It reads (Doligalski *et al.*, 1994):

$$\frac{\psi}{U_0 a} = (1-\alpha)Y + (1-\alpha)\ln\frac{X^2 + (Y-1)^2}{X^2 + (Y+1)^2} \tag{3}$$

Here $X = x/a$, and $Y = y/a$. After differentiating this to Y ($u = \partial\psi/\partial y$), and substituting $Y = 0$, we obtain an expression for the velocity at the wall, again in a frame of reference moving with the vortex:

$$\frac{u_w}{U_0} = (1-\alpha)\left(1 - 4\frac{1}{X^2+1}\right) \tag{4}$$

The pressure gradient can now be obtained by using: $\frac{\mathrm{d}p}{\mathrm{d}x} = -\rho u_w \frac{\partial u_w}{\partial x}$, as for the moving frame
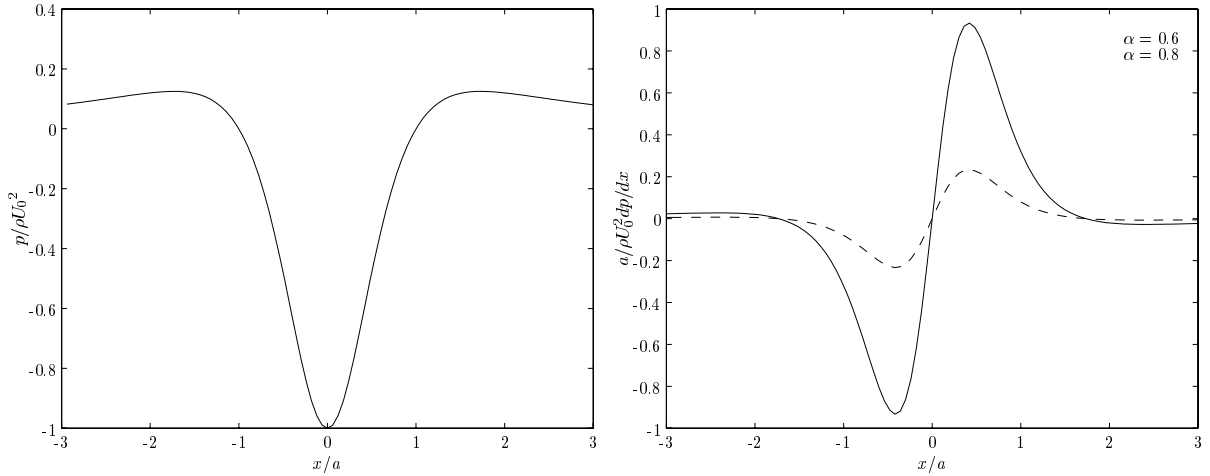
10

Figure 2: Pressure (left) and pressure gradient induced on boundary for two values of α (right)

of reference $\frac{\partial u_{\mathrm{w}}}{\partial t} = 0$. We now obtain:

$$\frac{a}{\rho U_0^2} \frac{\mathrm{d}p}{\mathrm{d}x} = -8 \frac{\left(X^2 - 3\right)\left(\alpha - 1\right)^2 X}{\left(X^2 + 1\right)^3} \tag{5}$$

The pressure and pressure gradient on the wall as a function of x/a are plotted in figure 2. It can be seen that left of the centre of the vortex a negative pressure gradient is induced by the vortex. This pressure gradient creates drag forces on a stone placed at that position, as the pressure on the upstream side of the particle is higher than on the downstream side in this area. Note that this is in contradiction with the quasi-steady mechanism, as u is decreased under the eddy. A vortex rotating in the opposite direction might therefore be better suited in creating extreme forces on a particle.

The absolute value of the pressure is more related to the lift force. If we regard an eddy at the distance of about half a stone diameter from the bed, then we can see that, when the eddy is above the particle, the pressure on the sides, and therefore also under the particle, is high, while the pressure on the top of the particle is low. This gives a large pressure gradient and can cause a high lift force. Below a further explanation follows of the relation between TWPs and forces on a bed particle.

4.2   Research on TWPs

Wall-pressure research is mainly aimed at other fields of application, like naval and acoustical applications; yet a lot of aspects –like pressure scaling laws, measuring equipment used, and data-processing techniques– are of interest to the present research.

11

As can be seen from the Poisson equation, TWPs in an incompressible fluid are caused by all velocity fluctuation gradients in the fluid domain at a certain moment. Therefore in principle the TWPs originate in the whole fluid domain, although the contribution of a single source does decrease with distance from the wall. It can be seen that different regions of the pressure spectrum are influenced by sources from different regions. In general lower frequency TWPs are caused by larger scale fluctuations further away. The pressure gradients can also be described by the local velocity plus acceleration, as described by the Navier-Stokes equation.

A number of power-laws have been predicted for the power spectrum of the TWPs under an equilibrium boundary layer flow. This is the standard flow situation, which is examined most often. Some of the power laws have also been measured (Gravante *et al.*, 1998; Farabee & Casarella, 1991). In the low frequency range the spectrum collapses on outer variables boundary layer thickness δ (which would be water depth, h in our case), and shear velocity u_*, although other variables are possible ($\overline{u}$ is proportional to u_*, for instance). In the mid region ($5 < \omega\delta/u_* < 100$) the spectrum is quite flat with a maximum at $\omega\delta/u_* \approx 50$. Farabee & Casarella (1991) state that the scaling behaviour in the low-frequency range will be different in channel flow, as the low-frequency pressures under an equilibrium boundary layer flow are probably determined by the rotational flow outside the developing boundary layer. The scaling variables used for the high frequency range are ν and u_*. A frequency range exists where the spectrum scales on both inner and outer variables ($100 < \omega\delta/u_*$ and $\omega\nu/u_*^2 < 0.3$). Here the spectrum decreases as ω^{-1}. The velocity sources of these pressures are thought to be situated in the log-region of the boundary layer. The width of this range increases with increasing Reynolds number. In the high frequency range ($0.3 < \omega\nu/u_*^2$), a power law according to $\omega^{-7/3}$ is predicted, but it has not clearly been measured. For the highest, viscosity dominated, frequencies, the pressures fall off according to the power law ω^{-5}.

Farabee & Casarella (1991) used their measurements together with the scaling laws above to predict the r.m.s. of the TWPs. As the ω^{-1} region grows with increasing Reynolds number, they proposed the following relation for the dimensionless r.m.s. of the TWPs, for Reynolds numbers ($Re_\delta = \delta u_*/\nu$) larger than 333:

$$\frac{\overline{p'^2}}{\tau_{\mathrm{w}}^2} = 6.5 + 1.86 \ln\left(\frac{u_*\delta}{333\,\nu}\right)$$

Only one paper was found which presented measurements of TWPs on a rough wall (Blake, 1970). Measurements were done under an equilibrium boundary layer on both smooth and rough walls. The scaling and shape of the spectrum appeared to be similar for both walls, with the distinction that the length scale that can be used to collapse the high-frequency part of the rough wall spectrum is the roughness height, k_g, instead of the viscous length scale (ν/u_*). The dimensionless frequency and spectral density, for which the high frequency part of the pressure spectra collapse are now: $\omega^+ = \omega\bar{k}_{\mathrm{g}}/u_*$ and $G_{\mathrm{pp}}^+(\omega^+) = G_{\mathrm{pp}}(\omega)u_*/\tau_{\mathrm{w}}^2\bar{k}_{\mathrm{g}}$. For the

low frequencies the wall pressures under a rough boundary layer flow show the same scaling behaviour as for the smooth wall. Also the influence of various spatial densities of roughness-elements was investigated. The spacing between the roughness elements is of influence to a lesser extent than the height. The r.m.s.-value of the pressure fluctuations (scaled by the dynamic pressure) was found to be roughly equal to that on smooth walls, although the value was different than found by later researchers.

Pressure fluctuations with a value of 4 times the standard deviation of the TWPs have been found in windtunnels (Schewe, 1983). Correlation of pressures with velocities did give clear origins for positive pressures. They can be seen to be located near shear layers with a velocity deficit, followed by fast moving flow. However, no clear velocity sources have been found for the negative pressures. All these results were obtained with smooth walls. In general the ratio of extreme values of any velocity derivative to its r.m.s. value is not constant in a turbulent flow, but increases with the global Reynolds number, although the exact determination of this effect is as of yet still difficult. This is very important for scaling flume-scale results to prototype situations.

Pressure gradients, rather than pressures, can create net forces on a stone. Therefore the relation between the two is of importance. The relation between a pressure spectrum and a pressure gradient spectrum is (George *et al.*, 1984, , for example): $G_{\Delta \mathrm{p} \Delta \mathrm{p}}(k) \propto k^2 G_{\mathrm{pp}}(k)$.

4.3 Pressure integration model

In section 4.1 an example is shown of a single vortex that induces wall pressures. Now we will examine whether the pressures that are inherent to a fully turbulent flow field could, in principle, lead to significant forces on a stone. Therefore we simply integrate a one dimensional pressure field over a spherical object, and see what magnitudes of drag force fluctuations result from it.

The model regards a stone in a stationary wall flow. The mean forces are not taken into account. Only the effect of a convecting, 'frozen' pressure field is determined. The assumptions are made that the pressure only varies in the flow direction, and that the pressure is not changed by the stone. The stone is schematised as a sphere. These assumptions lead to:

$$F'_{\mathrm{d,wp}}(k, \theta) = \int_{-R}^{R} p'(x, k, \theta) \frac{dA}{dx} dx$$

$$p'(x, k, \theta) = \hat{p}(k) \sin(kx + \theta) \tag{6}$$

$$A(x) = \pi(R^2 - x^2) \ \text{ for } |x| \leq R$$

Here $F'_{\mathrm{d,wp}}(k, \theta)$ is the drag force caused by the (Fourier) component of the fluctuating pressure, $p'(x, k, \theta)$. k is the wave number, $\theta = -U_{\mathrm{c}}kt$ is the phase, U_{c} is the convection velocity,

t is time, R is the radius of the stone, x is the longitudinal coordinate, and $A(x)$ is the cross-sectional area of the stone.

After substitution and solving the integral in eq. (6), the force becomes:

$$F'_{\text{d,wp}}(k, \theta) = 4\pi R^2 \hat{p}(k) \left(\frac{\cos(kR)}{kR} - \frac{\sin(kR)}{(kR)^2} \right) \cos(\theta) \tag{7}$$

This is the transfer function between p' and F'. In order to obtain some estimates of the variance of the drag force, caused by TWPs, we will use the gain factor from the pressure spectrum to the force spectrum:

$$|H_{\text{p,F}_{\text{d,wp}}}(k)| = \frac{\hat{F}}{\hat{p}} = 4\pi R^2 \left| \frac{\cos(kR)}{kR} - \frac{\sin(kR)}{(kR)^2} \right| \tag{8}$$

So, when a known TWPs spectrum is taken as a starting point, an estimate of the magnitude of the influence of the wall pressures on the drag force can be made by multiplying it by $|H_{\text{p,F}_{\text{d,wp}}}(k)|^2$.

Now we will examine whether TWPs can possibly influence stone stability directly in a prototype situation according to the model presented above. A uniform 'open channel flow' is chosen for this. The spectra in figure 3 show the TWPs under the uniform current and how the pressure spectrum is transformed into a spectrum of forces on a stone by eq. (8). The flow parameters are: depth-averaged flow velocity ($\overline{\overline{u}}$) is 2 m/s, water depth is 0.5 m, stone density is 2650 kg/m^3 and the Shields parameter is 0.04, from which it follows that the stone diameter (d) is 7 cm.

The TWPs spectrum for a rough wall (left plot of fig. 3) are obtained from Blake (1970). The low and high frequency fluctuations are scaled to prototype size (h is taken for δ), and the region in between is connected with a line of fixed exponent. The wall pressures for the wind tunnel flow are scaled to represent the flow parameters for the present case. Although an open channel flow has different turbulence characteristics than a zero pressure gradient channel flow, the pressure fluctuation characteristics for the mid and high frequency ranges –which scale with stone diameter and friction velocity– are expected to be similar, as they are generated by near bed flow processes, and the influence of a free surface on these is insignificant. For the low frequencies however, they are expected to differ, but they are used as no other information is available. For the transformation of the spectrum from ω to k, the relation $k = \omega / \frac{1}{2}\overline{\overline{u}}$ is used.

The middle and right plots show the gain factor, and the estimated force spectrum respectively, obtained from $G_{\text{F}_{\text{d,wp}}\text{F}_{\text{d,wp}}} = |H_{\text{p,F}_{\text{d,wp}}}(k)|^2 G_{\text{pp}}$.

The graphs in figure 3 demonstrate that especially the pressure fluctuations with wavelengths of the same order of magnitude as the diameter of the stone ($\lambda = 2\pi/k \approx 1.5\ d$, see dashed line in fig. 3) contribute to the forces on the stones and will hence be important for the determination of the stability of the stones. This agrees with the notion of Booij (1998). In
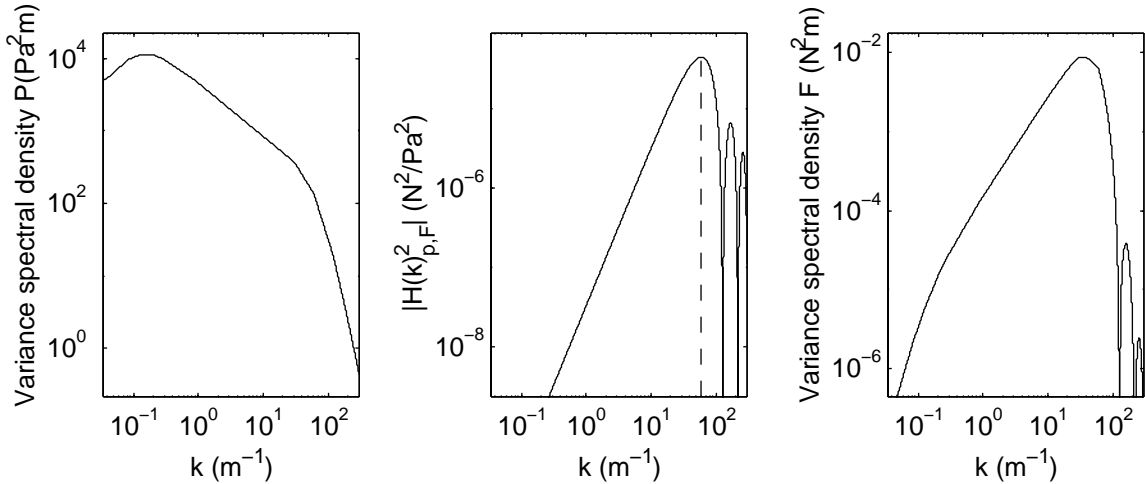
14

Figure 3: Autospectrum of pressures on rough bed (left), Gain factor squared (middle), and autospectrum of estimated forces

the low frequency range the transfer function rises with $\sim k^2$, which is the relation describing the relation between pressure and pressure gradient spectra.

When the power spectrum of the drag force is integrated, an estimation of the variance of the TWPs-induced drag force variations is obtained. In the present example three times the standard deviation of the drag force (an often used value for the 'maximal' occurring force) is equal to about 70% of the gravitational force on a stone. This means that the extreme values of the fluctuating forces calculated by the model are of the same order of magnitude as the average forces on the stone. Therefore it is likely that the forces that are directly generated by turbulence pressure fluctuations play a role and must be taken into account when regarding stone stability. Direct measurements of the forces on a stone, showed larger fluctuating drag forces, see for instance Xingkui & Fontijn (1993), so other mechanisms are also expected to increase the drag force.

The model still is highly idealised. For instance, at the moment only drag-forces are calculated. In principle the same approach is possible for the lift force, although the equivalent of eq. (7) does not allow the simple averaging over the phase. Furthermore, the effect of the stone on the pressure field is not taken into account. Experiments must show to which extent this is a valid assumption. Even so, the model indicates that the TWPs could give a significant contribution to the stability of stones. For now, this was only shown for a uniform flow, but for flow configurations with a relatively large turbulence intensity, the relative contribution of the fluctuating forces compared to the average forces can be expected to increase. The model also shows that the length scale of the turbulence fluctuations relative to the stone diameter

15

is of influence. The length scale should therefore be incorporated in stability models.

4.4   Behaviour in time

Now we regard the behaviour in time of the resultant force if a frozen pressure field is advected over a stone. This behaviour will be shown to decrease the stability of the stones. It also enables us to predict the shape of the normalised cross-correlation function, which we can compare to our measurements. In order to keep things simple we regard a two dimensional case. We take the definition of the pressure field as:

$$p' = \hat{p} \sin(k\,x - \omega\,t) \tag{9}$$

The drag force per unit width on a rod with radius R becomes [similar to eq. (6)]:

$$F'_{\mathrm{d,wp}} = \int_{-R}^{R} p' \frac{\mathrm{d}y}{\mathrm{d}x}\,\mathrm{d}x = -C_{\mathrm{d,wp}}(\tilde{k}) \cos(\omega\,t) \tag{10}$$

$$C_{\mathrm{d,wp}}(k) = 4\hat{p}R^2\,\frac{\sin\tilde{k} - \tilde{k}\,\cos\tilde{k}}{\tilde{k}^2} \tag{11}$$

where $\tilde{k} = kR$. The lift force, with the pressure in the lower half of the circle assumed constant over time and space, is:

$$F'_{\mathrm{l,wp,1}} = -\int_{-R}^{R} p'\,\mathrm{d}x = C_{\mathrm{l,wp,1}}(\tilde{k}) \sin(\omega\,t) \tag{12}$$

$$C_{\mathrm{l,wp,1}}(\tilde{k}) = 2\hat{p}R\,\frac{\sin\tilde{k}}{\tilde{k}} \tag{13}$$

This can be compared to the case where the pores are small or filled with finer material. When the pressure is assumed to be linearly changing under the lower hemisphere, more like an open granular structure, then the lift force becomes:

$$F'_{\mathrm{l,wp,2}} = -\int_{-R}^{R} p'\,\mathrm{d}x + R\,(p'(-R) + p'(R)) = C_{\mathrm{l,wp,2}}(\tilde{k}) \sin(\omega\,t) \tag{14}$$

$$C_{\mathrm{l,wp,2}}(\tilde{k}) = 2\hat{p}R\,\left(\frac{\sin\tilde{k}}{\tilde{k}} - \cos\tilde{k}\right) \tag{15}$$

The factors $C_{\mathrm{d,wp}}$, $C_{\mathrm{l,wp,1}}$ and $C_{\mathrm{l,wp,2}}$ are all positive for $0 < k < \pi$. Which means that for wavelengths larger than the stone diameter $(2R)$ the force-vector will rotate in time, along an ellipsoidal path, with semi-axes equal to the amplitudes of the lift and drag forces, as given by eqs. (10) to (15). In figure 4 the time variation of the resultant force is illustrated for a sinusoidal pressure field advected over a stone. This behaviour is increasing the efficiency in
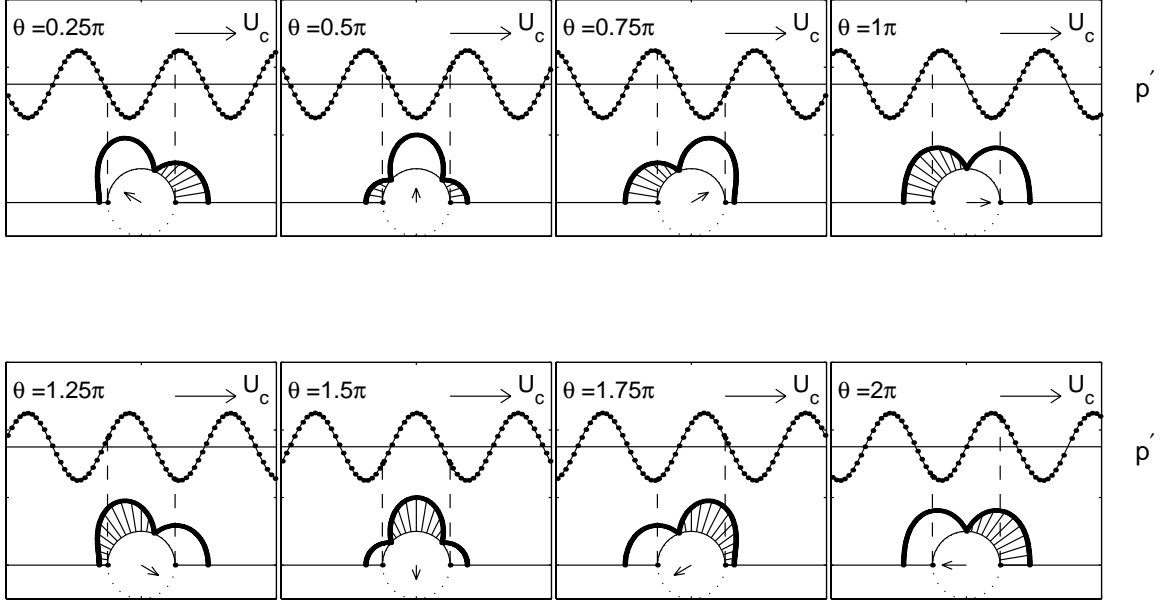
16

Figure 4: Change of the integrated force on a particle due to a convected frozen pressure field for $\lambda/d = 1.5$. Hatched pressure field: positive pressure, blank pressure field: negative pressure. The vector in the stone represents the resulting net force acting on the stone.

which this force can dislodge a particle. First of all, the force vector covers all directions, including the direction where it generates the largest moment around the angle of repose of the grain. Secondly, the direction of the force will "follow" this angle. Because, as the particle rolls over its downstream contact point, the angle of repose, ϕ, will become smaller, which will change the optimal angle for creating the largest moment around the point of contact in exactly the same direction in which the fluctuating force is moving. This will increase the duration of time during which the maximal moment is exerted on the stone.

In order to see whether the temporal behaviour of the force vector is observed in our measurements, we will now derive the theoretical shape of the normalised cross covariance function between drag and lift, $\rho_{\mathrm{dl,wp}}$, which will be compared later to ρ_{dl}, estimated from the measured pressures. $\rho_{\mathrm{dl,wp}}$ can be derived from the definition of the normalised cross covariance function:

$$\rho_{\mathrm{dl,wp}}(\tau) = \frac{\lim_{T \to \infty} \frac{1}{T} \int_0^T F_{\mathrm{d,wp}}(\omega\, t)\, F_{\mathrm{l,wp}}(\omega\,(t+\tau))\, \mathrm{d}t}{\sigma_{\mathrm{d}}\sigma_{\mathrm{l}}} = -\sin\omega\,\tau \qquad (16)$$

17

where σ_i is the standard deviation of force i. The turbulence field is obviously not a sine as used for the derivation of the force-functions. Therefore $\rho_{dl,wp}$ has to be multiplied by the loss of correlation of the wall pressures itself. When the autocorrelation function of wall pressures, γ, is assumed to be exponential, it yields: $\gamma^{\left(\frac{k}{2\pi}|x|\right)}$. We further substitute $U_c\tau$ for x, and kU_c for ω and we obtain:

$$\rho_{dl,wp}(\tau) = -\sin(U_c\,k\,\tau)\,\gamma^{\left(\frac{kU_c}{2\pi}|\tau|\right)} \tag{17}$$

It can be seen that the value of C_d or C_l is lost in this formulation, which makes it easier to compare this shape to measurements. The function is shown in figure 5 for the values $\gamma_\lambda = 0.005$, $U_c = 0.2$ m/s, and $k = 2\pi/0.12$ m^{-1}, together with the measured ρ_{dl}, for all measured configurations. The graphs will be discussed below.

4.5   Extraction of extreme values

It is logical to look at the origin of the extreme values of the pressure gradients, as especially the extreme forces are of interest for low-mobility transport. For the quasi-steady forces we expected a maximal u velocity to correspond to a maximal drag force, and a combination of $+u'$ and $-v'$ to be related to maximum lift force. We will now derive which velocity fluctuations near the stone could indicate extreme forces, if caused by the TWPs.

For the evaluation of the velocity sources of the potential forces we start out with the Euler equation (Navier-Stokes equation without viscosity).

$$-\frac{1}{\rho}\nabla p = \frac{\mathrm{D}\vec{u}}{\mathrm{D}t} = \frac{\partial\vec{u}}{\partial t} + (\vec{u}\cdot\nabla)\vec{u} \tag{18}$$

Next we apply a Reynolds decomposition. Because of the fact that it is an open channel boundary layer flow over a flat bed (regarded on a length scale exceeding the roughness size), V, W, $\frac{\partial U}{\partial x}$, and $\frac{\partial U}{\partial z}$ are zero. Therefore a number of terms drops out. The non linear terms $(\vec{u'}\cdot\nabla\vec{u'})$ are not completely insignificant, as near the bed the extreme values of u' are of the order of U. It can be argued however, that they are smaller than the terms with mean values: $u' < U$ is still valid, and, as we regard the extreme values, $\frac{\partial u'}{\partial x}$ and u' do not have their maximum values at the same time. The last reason mentioned does not hold for the nonlinear terms with v' and w' (v' can very well have its maximum at the same time as $\frac{\partial u'}{\partial x}$) , but in general $|w'| < |v'| < |u'|$. Therefore they are omitted as well, although their unimportance is not completely certain. The fluctuating part of the horizontal pressure gradient finally becomes:

$$-\frac{1}{\rho}\frac{\partial p'}{\partial x} \approx \frac{\partial u'}{\partial t} + U\frac{\partial u'}{\partial x} + v'\frac{\partial U}{\partial y} \tag{19}$$

Not all the terms in eq. (19) have been measured. If we would try to use a form of the Taylor hypothesis (a "frozen" turbulence field is convected by the mean velocity: $\frac{\partial u}{\partial x} \approx -\frac{1}{U}\frac{\partial u}{\partial t}$), in order to end up with terms that have been measured, the first two terms of equation (19)
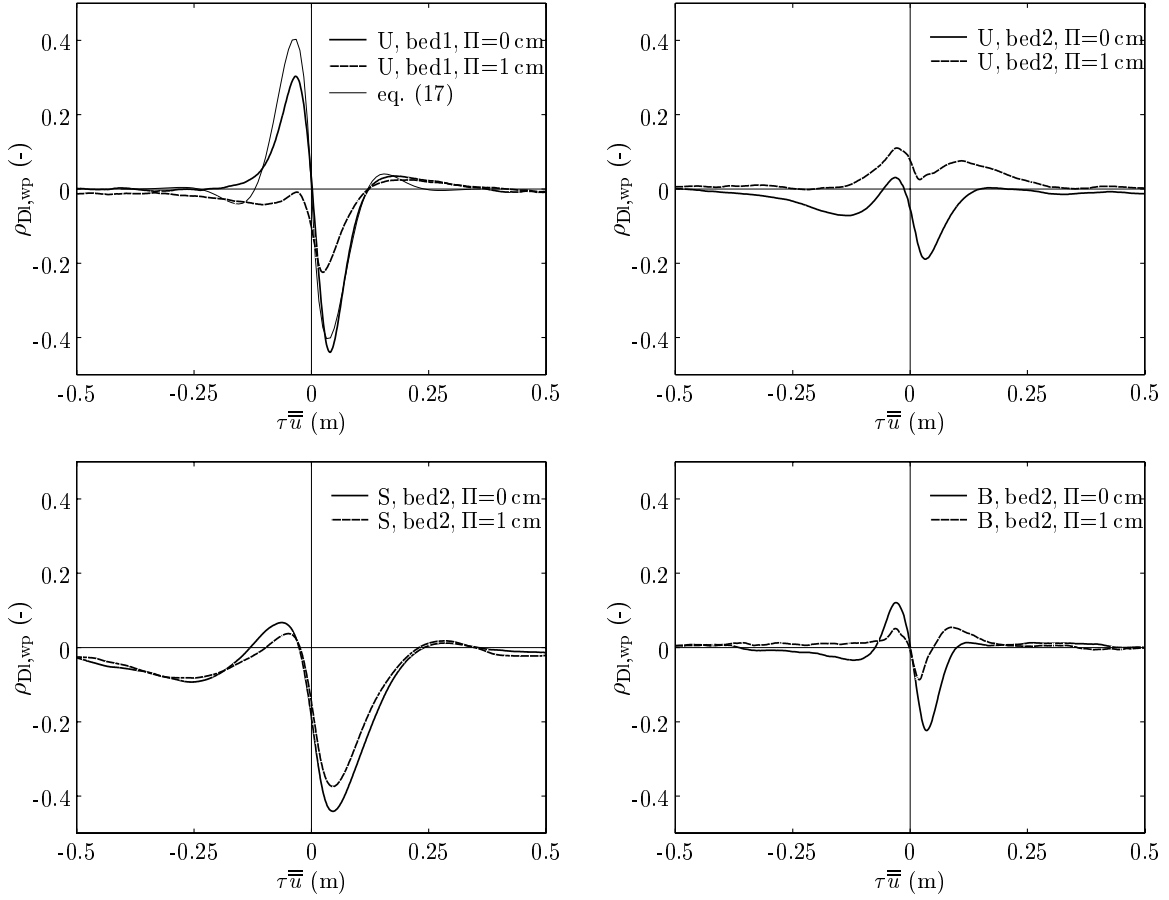
18

Figure 5: Measured correlations $\rho_{\mathrm{dl,wp}}$ for configurations U,B, and S.

become: $\frac{\partial u'}{\partial t} + U\frac{\partial u'}{\partial x} \approx 0$. This means that if in a frame of reference moving with the mean velocity, U, the flow field would not change in time, and these terms do not induce pressure fluctuations. As they do change in time (Blake, 1970) a point measurement cannot give information about the magnitude of the influence of these terms. Therefore we need spatially distributed measurements in order to evaluate all terms in the right hand side of eq. (19). Only the term $-v'\frac{\partial U}{\partial y}$ has been measured with the present one-point, two-component LDV set-up. If we combine eq. (19) and the expression for the force on a body of volume V in a pressure field with a linear gradient, we obtain:

$$\Delta p'_{\mathrm{D}} \propto F_x = -V\frac{\partial p}{\partial x} \propto v'\frac{\partial U}{\partial y} + \frac{\mathrm{D}u'}{\mathrm{D}t} \tag{20}$$

The first term on the right hand size of eq. (20) has been measured and we can check whether extreme values of this term occur simultaneous with extreme values of $\Delta p'_{\mathrm{D}}$. The material derivative has not been measured.

A similar derivation for the vertical pressure gradient results in the following expression for the fluctuating lift force induced by TWPs:

$$\Delta p'_{\mathrm{L}} \propto \rho\frac{\mathrm{D}v'}{\mathrm{D}t} \tag{21}$$

The right hand side of this equation cannot be evaluated from the present measurements.

The most effective fluctuating pressures of this kind are expected to have spatial dimensions in the order of twice the stone size (Booij, 1998, and section 4.3), which have a high frequency compared to the quasi-steady fluctuations. The pressure gradient diminishes rapidly at a certain distance from an eddy, so only correlation with velocities close to the stone can be expected.

From the above we can conclude that if high frequency, positive v-fluctuations correspond to increased Δp_{D}, then this indicates that the TWPs induced force fluctuations are responsible for a part of the variance of the fluctuating drag force. The material derivatives of u' and v', which can also cause potential forces, cannot be measured. Only the significance of the drag component caused by the TWP can be regarded from a one-point measurement. However, if this force component is present it will indicate that TWPs-induced lift is present as well, because if the pressure field is convected over the stone, the typical sequence of different force components (section 4.4) must be present as well.

5 Measurements

5.1 Set-up

A flume was used of 14 m long, 0.5 m wide and 0.6 m high. The water was led into the flume through a stilling basin. The flow from the stilling basin caused a wavy water surface in the
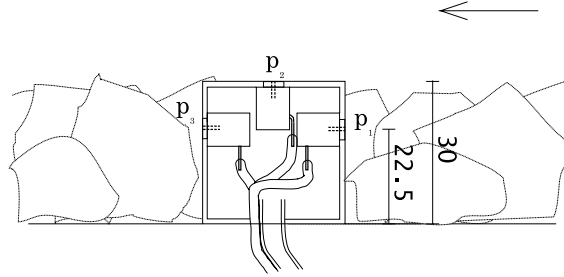
Figure 6: Longitudinal section of the instrumented cube (model stone) including three pressure transducers

flume. The waves were damped by a floating polystyrene plate near the inflow. A cavity was present under the measuring section. A removable lid on the cavity was used to fix the model stone. The lid could be removed with the surrounding stones on it, so that the local stone topography could be kept unchanged. In the cavity itself one pressure sensor was placed, to measure the spurious pressures generated by environmental vibrations of the flume. Stones were placed on the floor manually, one layer thick, from 5 m upstream to 2 m downstream of the model stone.

A cubical shape was chosen for the model stone for a number of reasons. It has sharp edges like crushed stone used for bed protections, it is easy to describe, and the flow around it is fairly easy to analyse. The orientation of the cube was such that one face was placed on the bed, and two side faces were parallel to the flow direction. A 30 mm high, hollow cube was welded from 1.5 mm thick stainless steel. Pressure transducers were installed in three faces, see figure 6. They were all mounted in the central axis of the flume. The transducers at the upstream (p_1) and downstream side (p_3) were placed at $\frac{3}{4}d$ from the bed, and the top sensor (p_2) was placed in the middle of the top face of the cube. The electrical wiring and a tube connected to the atmosphere reference pressure were led through the bottom of the cube to the cavity under the bed. The hole through which the wiring was led was sealed off as well to keep the inside of the cube dry with an atmospheric reference pressure. It was possible to move the cube to different vertical positions, enabling different protrusions and orientations.

The stones were standard stones used in the Fluid Mechanics Laboratory. According to the classification of the CUR-manual (CUR, 1995) the stones can be classified as being shaped irregularly (IR). The roundness of the stones is low, i.e. the edges are sharp. The rocks were sieved with two sieves with openings of respectively 2.5 cm and and 4 cm, in order to get a shortest axis (which point upwards) of about 3 cm length, corresponding to the size of the cube. Extremely elongated or tabular stones were removed. Still quite some variation was present in the heights of the stones. The stones were placed one by one on the floor, without the use of adhesives. The flow velocity in the experiments was too low to displace them.

Miniature, low-range, piezo-resistive pressure transducers were used to capture the fluc-
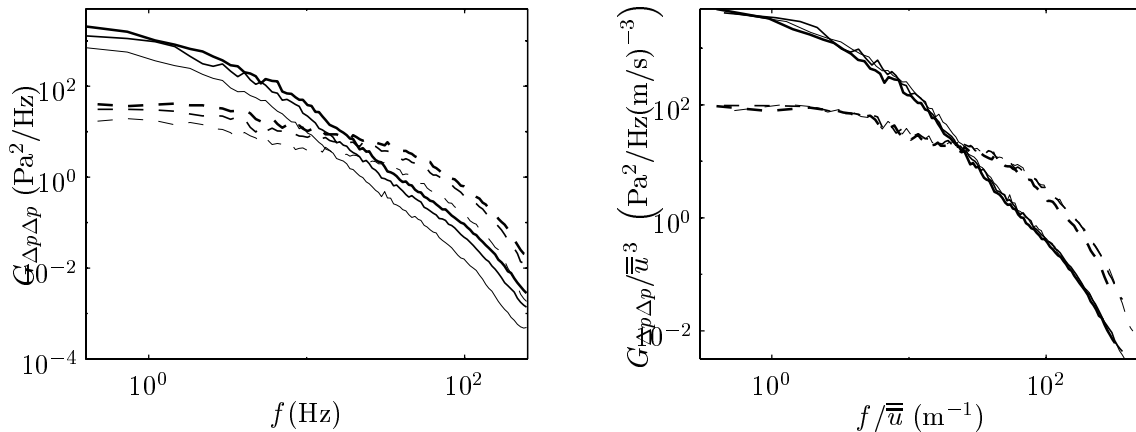
Figure 7: Example of pressure spectra on cube. Both in real dimensions (left), and normalised with $\overline{\overline{u}}$ (right). Configuration: bed 2 and $\Pi = 1$ cm. Parameters: $Q = 65/55/45$ l/s; a thinner line means a lower Q. Solid line: $G_{\Delta p_{\mathrm{D}} \Delta p_{\mathrm{D}}}$, dashed line: $G_{\Delta p_{\mathrm{L}} \Delta p_{\mathrm{L}}}$.

tuating pressure fluctuations. They are manufactured by *Honeywell* (type 24pcefa1d). The transducers have a full scale range of 3450 N/m, a response time of < 1 ms, and a maximum error due to repeatability, hysteresis and linearity of 0.4 %. The dimensions of the polyetherimide housing are 6 mm $\times$ 9 mm $\times$ 7 mm, and the dimensions of the measuring diaphragm are 2 mm $\times$ 2 mm. The opening between sensor and cube was sealed with a two-component epoxy resin, so that only the positive side of the diaphragm was exposed to the surrounding water. The transducers have a rather large temperature-dependence, but as the temperature in the flume is very nearly constant (within 0.1°C), this was hardly of influence.

A 4 mW 'Laser Doppler Flow Meter' made by WL|Delft Hydraulics was applied for the velocity measurements. It uses the forward-scatter, reference-beam method. The front lens with a 400 mm focal distance generates a measuring volume with dimensions of about 10 mm horizontally normal to the flow, and 1 mm in the other directions. Measurements were done 1 cm upstream of the cube. The laser could be traversed up and down. Measurements described here are taken at $y \approx 15 \pm 1.5$ mm, above the top of the cube with protrusion, $\Pi = 0$ cm.

A Pitot tube was installed at three positions in the flume in order to measure the water level, using only the (hydro-) static pressure. The reproducibility of a measurement was within 0.2 mm. The accuracy of one water level measurement is estimated at 0.4 mm. The discharge was measured by an orifice plate was installed in the inflow pipe with an accuracy of about 0.7 l/s.

Config.	bed #	Π [cm]	Q $[\frac{\mathrm{m}^3}{\mathrm{s}}]$	h [m]	Re [-]	Re_* [-]	τ_w $[\frac{\mathrm{N}}{\mathrm{m}^2}]$	$\overline{\Delta p_{\mathrm{D}}}$ $[\frac{\mathrm{N}}{\mathrm{m}^2}]$	$\Delta p'_{\mathrm{D,rms}}$ $[\frac{\mathrm{N}}{\mathrm{m}^2}]$	$\Delta p'_{\mathrm{L,rms}}$ $[\frac{\mathrm{N}}{\mathrm{m}^2}]$	$\frac{\Delta p'_{\mathrm{D,rms}}}{\Delta p'_{\mathrm{L,rms}}}$ [-]
U	1	0	0.065	0.168	$1.3 \cdot 10^5$	3250	11.3	25	17.4	14.4	1.21
U	1	1	0.065	0.166	$1.3 \cdot 10^5$	3250	11.8	98	57.9	19.3	3.00
U	1	0	0.055	0.161	$1.1 \cdot 10^5$	2650	7.6	29	14.1	12.7	1.11
U	1	1	0.055	0.159	$1.1 \cdot 10^5$	2650	7.5	85	49.2	16.9	2.91
U	1	0	0.045	0.157	$0.9 \cdot 10^5$	2200	5.2	25	10.0	9.1	1.10
U	1	1	0.045	0.156	$0.9 \cdot 10^5$	2200	5.5	70	35.6	11.2	3.17
U	2	0	0.065	0.169	$1.3 \cdot 10^5$	3250	12.1	71	43.6	14.9	2.92
U	2	1	0.065	0.167	$1.3 \cdot 10^5$	3250	12.3	145	68.4	24.1	2.83
U	2	0	0.055	0.162	$1.1 \cdot 10^5$	2650	10.9	69	31.3	11.1	2.83
U	2	1	0.055	0.157	$1.1 \cdot 10^5$	2650	6.9	110	56.5	19.8	2.86
U	2	0	0.045	0.156	$0.9 \cdot 10^5$	2200	5.8	55	26.2	9.8	2.66
U	2	1	0.045	0.154	$0.9 \cdot 10^5$	2200	4.4	86	38.2	13.9	2.75
B	2	0	0.055	0.160	$1.1 \cdot 10^5$	2600*	7.6*	43	22.6	9.1	2.48
B	2	1	0.055	0.159	$1.1 \cdot 10^5$	2600*	7.5*	137	44.4	18.6	2.38
S	2	0	0.035	0.201	$0.7 \cdot 10^5$*	–*	–*	-15	13.8	10.4	1.32
S	2	1	0.035	0.200	$0.7 \cdot 10^5$*	–*	–*	15	18.7	11.4	1.64

Table 1: Flow conditions, and mean parameters for the three configurations.

5.2 Experimental configurations and conditions

Several configurations were considered. First a uniform open channel flow was examined (case U) with two different bed-configurations. Each bed was made with the same stones, placed with the same density. Only the micro-topography around the cube was changed due to the random placement of the stones. After that the second bed-configuration was used with a backward-facing step upstream of the cube (case S), so that the cube was about four water depths downstream of the reattachment point. For the third configuration, again with the same bed-configuration as case S, stones were removed upstream of the cube, so that it was placed at the beginning of a rough bed (case B). In table 1 the flow conditions for the various configurations are mentioned.

In this report the following coordinate system is used: the x-axis is chosen in the direction of the flume, directed downstream. The y-axis is directed vertically upward, and the z-axis is directed in the transverse direction. Indicators for the potentially displacing fluctuating drag and lift forces are obtained from the measured pressures by $\Delta p_{\mathrm{D}} = p_1 - p_3$ and $\Delta p_{\mathrm{L}} = -p_2$, respectively.

In figure 8 the average velocity profiles, Reynolds stress, and turbulence intensities for the three configurations are presented, normalised by the mean velocity. The determination of the average forces was rather imprecise. Because the pressure sensor reading had an unknown offset due to the amplification of the signal, the mean pressure was determined by measuring
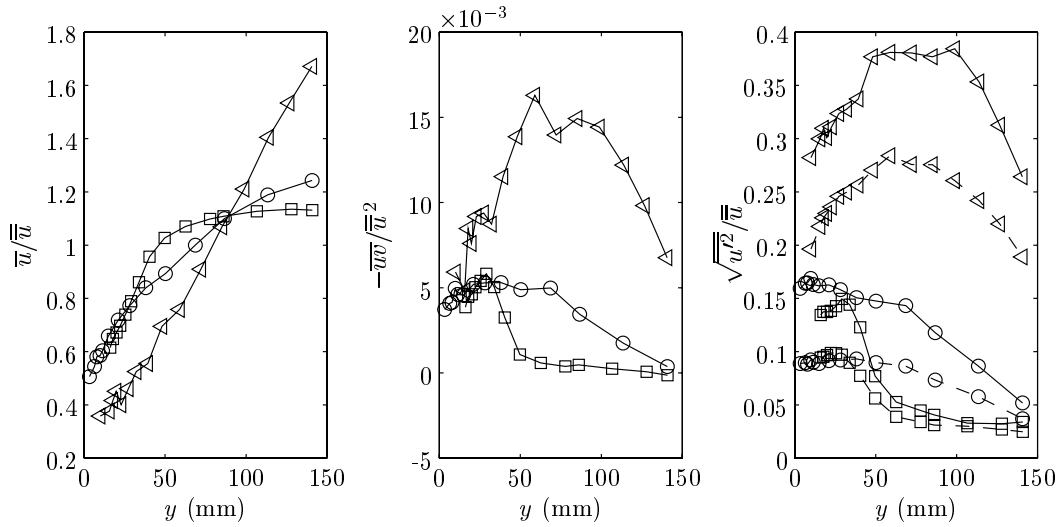
Figure 8: Vertical profiles of mean flow (left), Reynolds stress (middle) and turbulence intensity (right, u-component: solid line, v-component: dashed line) normalised by $\overline{\overline{u}}$ for configurations U ($\circ$), B ($\square$), and S ($\triangleleft$).

the pressure difference before and after stopping the flume together with the water level before and after. This gave a combination of several error sources. The shear stress was determined with the following equation:

$$\tau = \rho(\beta\overline{\overline{u}}^2 - gh)\frac{\Delta h}{\Delta x} \tag{22}$$

The term $\beta\overline{\overline{u}}^2\frac{\mathrm{d}h}{\mathrm{d}x}$ is caused by the fact that the flume has a horizontal bed. The ratio between depth averaged momentum flux and momentum flux based on depth averaged velocity, β, which is used in eq. (22), was determined from a log-fit through the measured velocity profile at 1.06, for the uniform flow.

Both $\overline{\Delta p_{\mathrm{D}}}$, $\overline{\Delta p_{\mathrm{L}}}$ and τ_{w} could not be measured with a great accuracy, therefore $\overline{\overline{u}} = Q/Bh$ is used as a scaling variable for the pressures, when we want to check whether the flow is fully rough.

6   Uniform flow (case U)

The fluctuating pressures Δp_{D} and Δp_{L} were determined accurately. In figure 7, an example of spectra of both components are depicted for three discharges. As the length scales (depth and stone size) are the same in all cases, the spectra should collapse if the time scale is
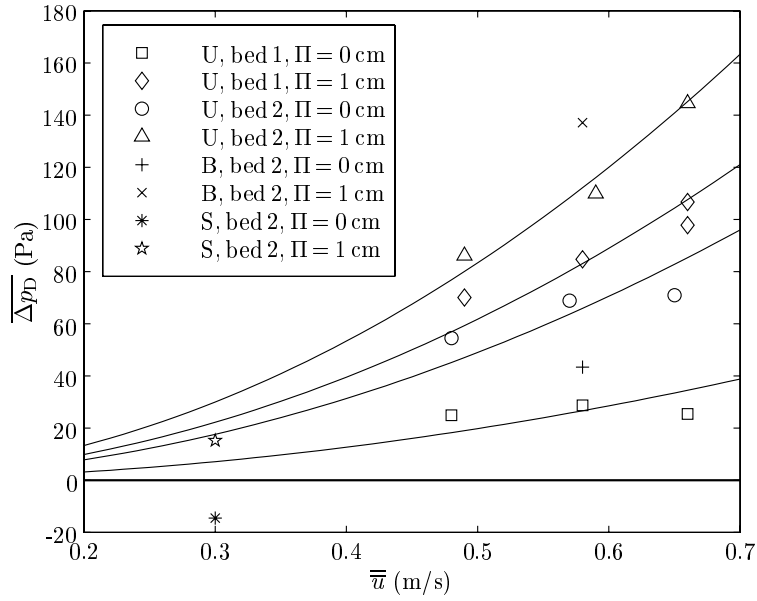
24

Figure 9: $\overline{\Delta p_{\mathrm{D}}}$ as a function of Q for all measurements. Lines are fits of $\alpha\,\overline{\overline{u}}^{\,2}$ through the points for the uniform flow.
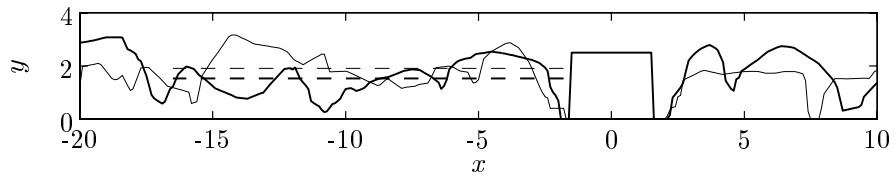

Figure 10: Longitudinal bed profile, averaged over cube width, for bed 1 (thin line) and bed 2 (thick line). Average level upstream of cube is indicated by the dashed lines. The cube ($\Pi = 0$) is situated at $x = 0$.

25

removed from the both axes. So G was divided by $\overline{\overline{u}}^3$, and f was divided by $\overline{\overline{u}}$. It can be seen that the spectra collapse well. Despite the imprecise determination of the mean pressure gradients, it can be seen that $\overline{\Delta p_{\mathrm{D}}}$ rises quadratically with increasing flow velocity (figure 9). For $\overline{\Delta p_{\mathrm{L}}}$, which was approximately 10 % of $\overline{\Delta p_{\mathrm{D}}}$, the relative error was too large, and no trend could be observed. Therefore it is not shown here.

6.1 Influence of protrusion

The protrusion is the height of the top of the stone related to a global mean bed level (for the bed level we chose the y coordinate where the porosity was 90%, which is the height of the top of the cube for $\Pi = 0$ cm). The protrusion is not the only factor that influences the forces on a stone, as the positions of the surrounding stones are also of importance. Still the protrusion can be expected to have a strong influence on the magnitude of the critical force, as it is related to both the resisting force of the particle (the angle of repose generally decreases with increasing protrusion), as well as to the hydrodynamic force acting on the particle (the exposed area increases with increasing protrusion).

A measure that is related more directly to the hydrodynamic load is the exposure, e, of the stone. The exposure is the height of the top of the stone related to the local, mean, upstream bed level. This distance is related to the exposed area of the stone and consequently it is related to the drag force. Therefore the drag force on the stone is expected to be influenced more directly by the exposure than by the protrusion, although on average Π will increase with increasing e. Thus, it is expected that if something is related to the exposure, it will also be related to protrusion, only with more scatter. If we define the exposure as the height of the top of the cube to the mean bed level between the cube and five cube side lengths in front it (see levels in figure 10), this results in the following exposures; for bed 1 $e = \Pi + 1.09$ cm, and for bed 2 $e = \Pi + 1.47$ cm. This means that the flow configurations in order of increasing exposure are: bed 1 & $\Pi = 0$cm, bed 2 & $\Pi = 0$cm, bed 1 & $\Pi = 1cm$, bed 2 & $\Pi = 1$cm. In figure 9 it can be seen that $\alpha = \overline{\Delta p_{\mathrm{D}}}/\overline{\overline{u}}^2$ goes up with increasing exposure, as often assumed (Egiazaroff, 1965, , for example), but –to our knowledge– never shown directly for a natural configuration.

6.1.1 Quadrant analysis

We will now do a quadrant analysis in order to investigate the dependance of the pressures on the instantaneous velocity (-fluctuation), on the basis of figures 11 and 12. The plots display isolines of the joint PDF of (u,v), as well as the conditionally averaged pressures, $\overline{\Delta p'_{\mathrm{D}}(u,v)}$ and $\overline{\Delta p'_{\mathrm{L}}(u,v)}$, which show the average pressure during a certain flow direction and
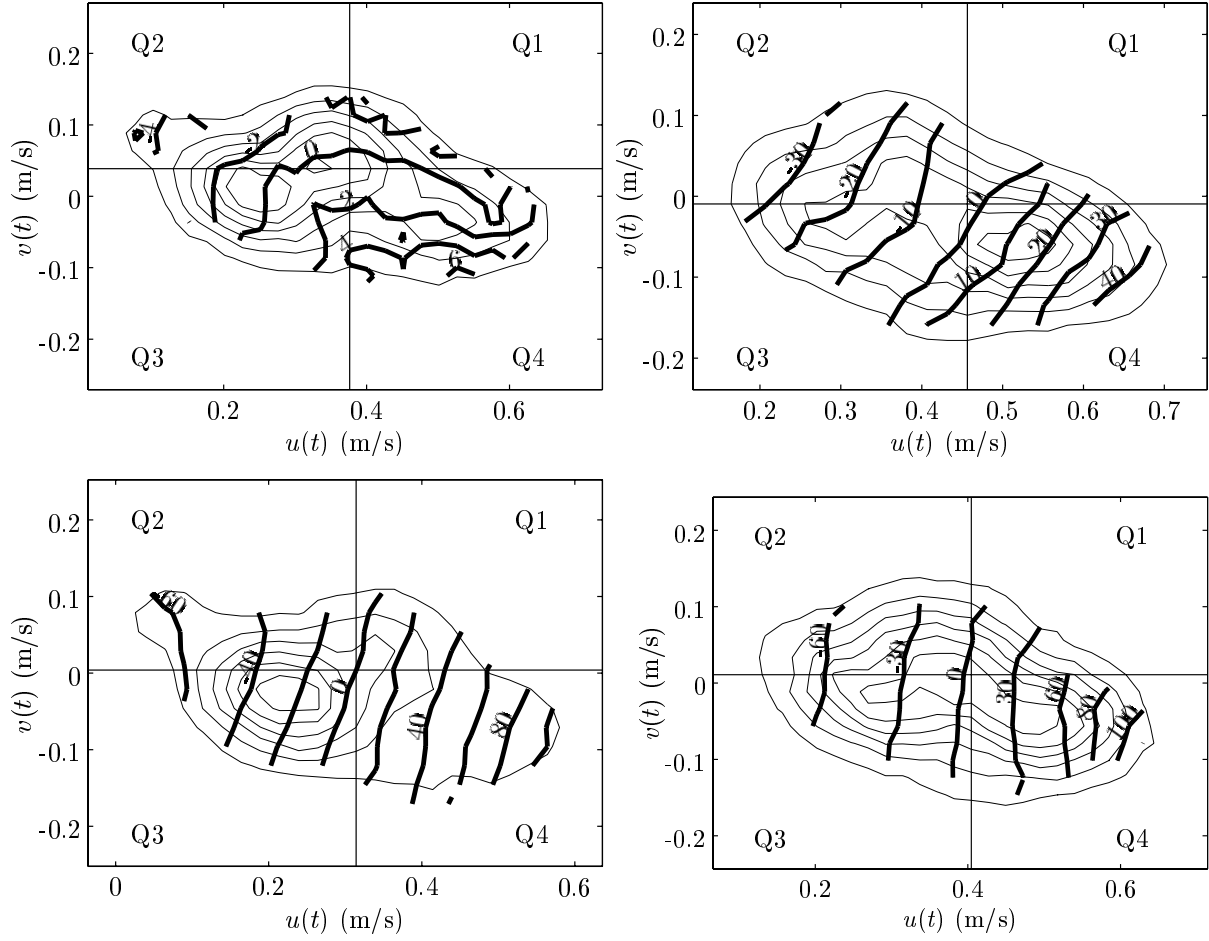
Figure 11: Joint probability density function of $u(t)$ and $v(t)$ (thin isolines), and conditionally averaged horizontal pressure gradient, $\overline{\Delta p'_{\mathrm{D}}(u, v)}$ (thick isolines, label units: Pa) for uniform flow (U). From left to right and from top to bottom respectively: bed 1 and $\Pi = 0$ cm; bed 2 and $\Pi = 0$ cm; bed 1 and $\Pi = 1$ cm; bed 2 and $\Pi = 1$ cm.
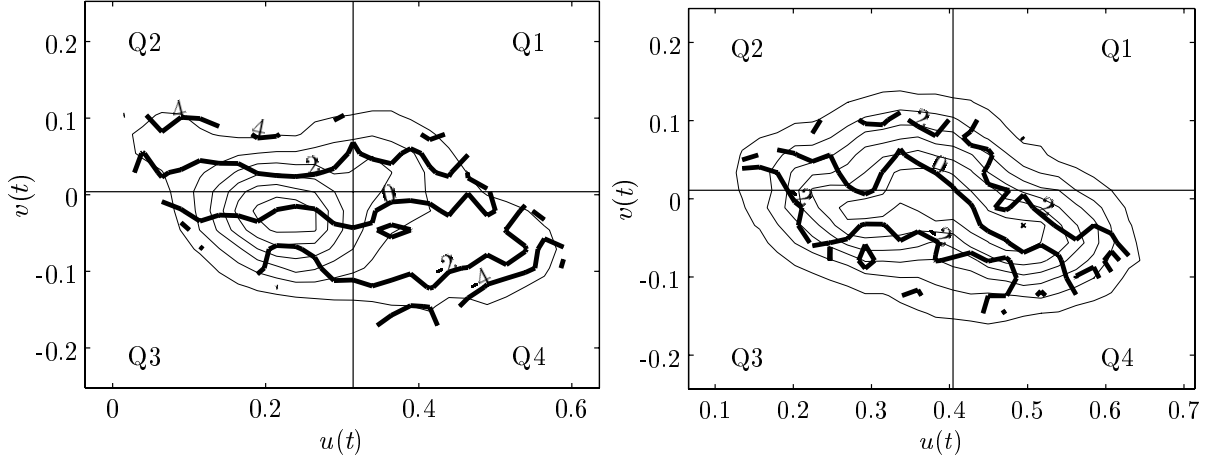
Figure 12: Joint probability density function of (u,v) (thin isolines), and conditionally averaged vertical pressure, $\overline{\Delta p'_{\mathrm{L}}(u,v)}$ (thick isolines) for uniform flow (U). Bed 1 (left) and bed 2 (right); $\Pi = 1$ cm.

magnitude. They are defined as:

$$\overline{\Delta p'_{\mathrm{c}}(u,v)} = \frac{1}{n_{\mathrm{i}}} \sum_{i \in S} \Delta p'_{\mathrm{c}}(i), \text{ where } S = i \mid -\tfrac{1}{2}w < u(i) - u \leq \tfrac{1}{2}w \ \wedge \ -\tfrac{1}{2}w < v(i) - v \leq \tfrac{1}{2}w$$

(23)

where i is the sample number, c is D or L, w is the bin width and n_i is the number of measurements within a bin.

In figure 11 $\overline{\Delta p'_{\mathrm{D}}(u,v)}$ is depicted for increasing exposure. For the various exposures it can be seen that the gradient of the $\overline{\Delta p'_{\mathrm{D}}(u,v)}$ surface has a fairly constant direction over all (u,v) combinations. For the most exposed particle (bed 2, $\Pi = 1$cm), $\overline{\Delta p'_{\mathrm{D}}(u,v)}$ is hardly dependent on v, simply a higher $u^{(2)}$ gives increased $\overline{\Delta p'_{\mathrm{D}}(u,v)}$. This will still lead to a situation where most extreme forces occur during Q_4 events, simply because the events with highest u occur in this quadrant. When the exposure decreases it can be seen that $\overline{\Delta p'_{\mathrm{D}}(u,v)}$ becomes a function of vertical velocity as well. This was not expected at first, but can be explained by the fact that, when the stone is shielded by upstream stones, a downward flow is necessary to let the flow reach the stone. The stone must obstruct the flow to give the flow a curvature, which will cause the pressures on the stone to change. For the least exposure (where the cube is almost totally shielded by the upstream stones, see figure 10) the dependence of $\Delta p'_{\mathrm{D}}$ on the longitudinal velocity is almost totally gone, and it is almost totally dependent on vertical velocity. We must keep in mind that we have only measured a point pressure. Therefore for a certain stone this effect will probably be different for various heights of the stone. But it shows that Q_4-events are not only the source of increased transport because they occur more
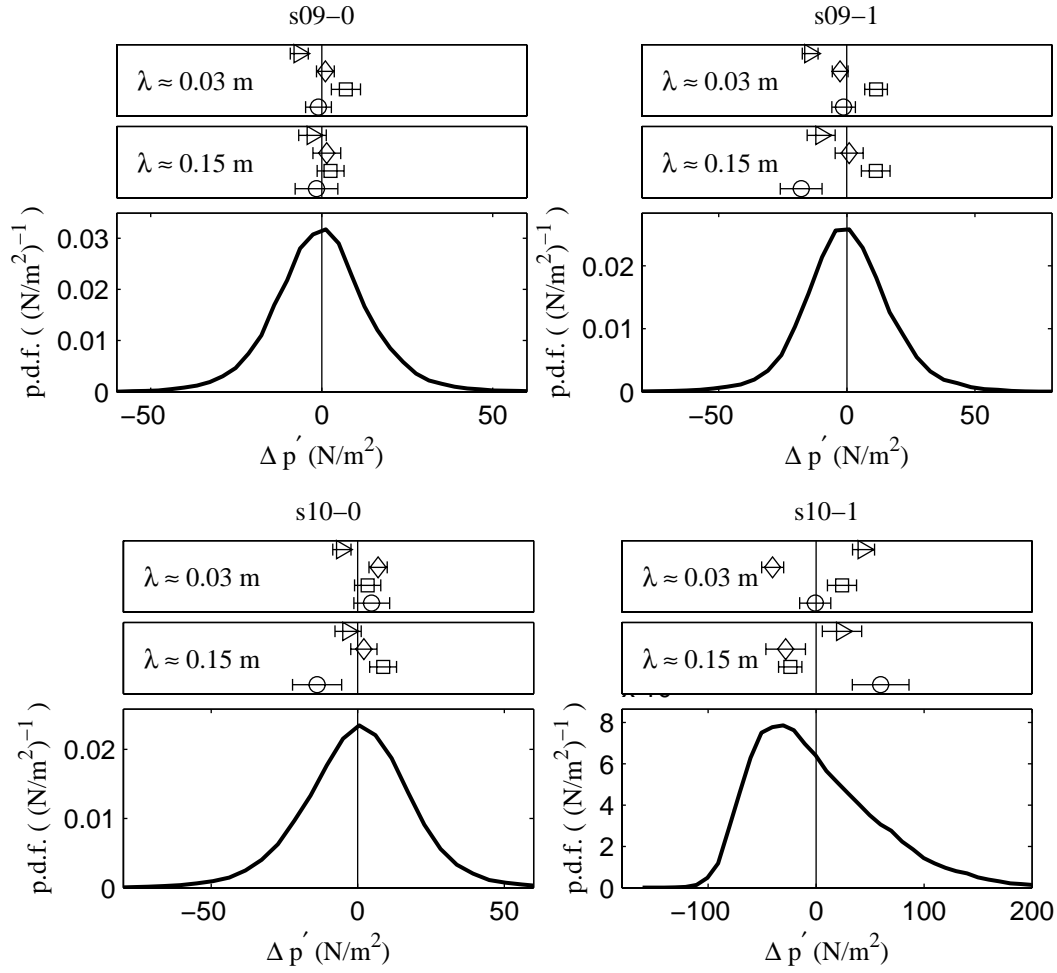
28

Figure 13: PDFs of $\Delta p'_L$ (left) and $\Delta p'_D$ (right) for U configuration, $\Pi = 0$ (top) and $\Pi = 1$ cm (bottom). The (horizontal position of the) markers in the panels on top represent $\widehat{\Delta p'_D}$ and $\widehat{\Delta p'_L}$ for two band-pass filtered signals of $-uv_{Q2}$ ($\triangleright$), $-uv_{Q4}$ ($\diamond$), $+v$ ($\square$), and $+u$ ($\circ$), at centre frequencies corresponding to $\lambda \approx 0.03$ m, and $\lambda \approx 0.15$ m.
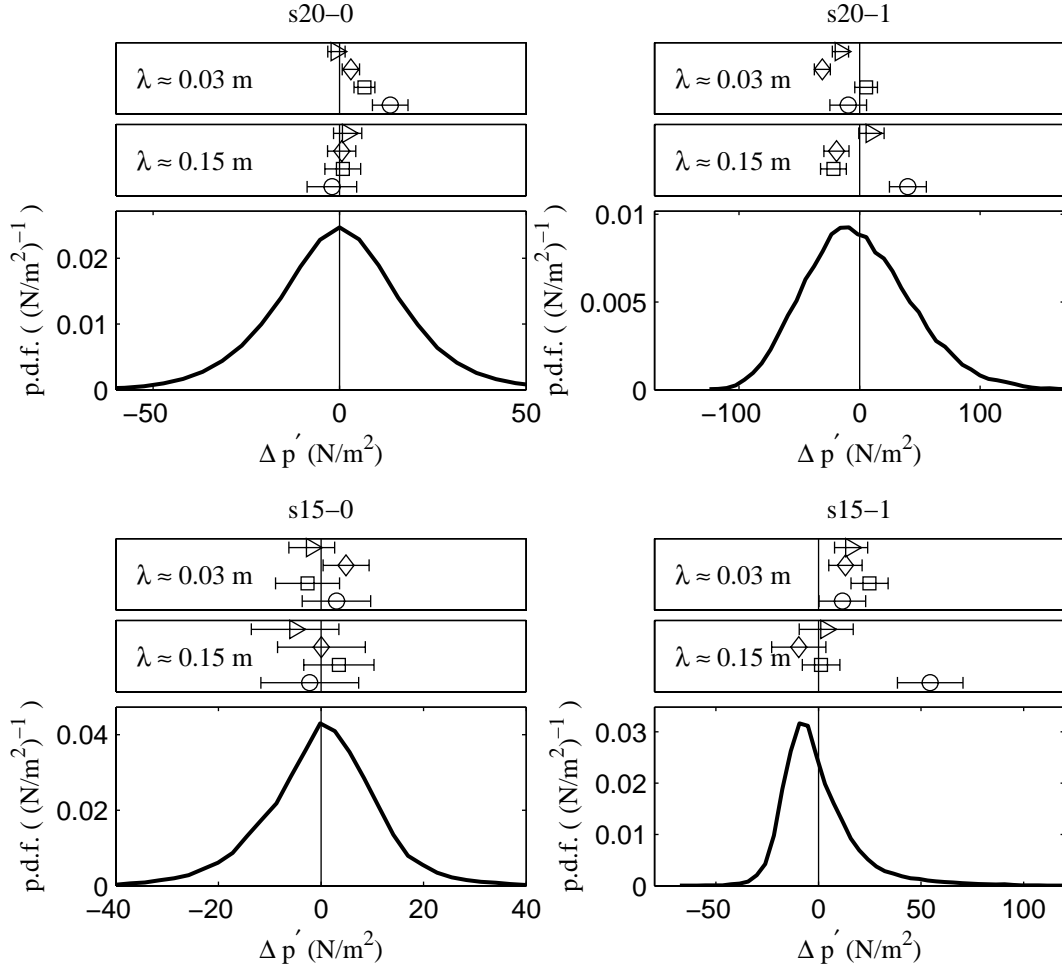
29

Figure 14: PDFs of $\Delta p'_L$ (left) and $\Delta p'_D$ (right) for B (top) and S (bottom) configurations; $\Pi = 1$ cm. The (horizontal position of the) markers in the panels on top represent $\widehat{\Delta p'_D}$ and $\widehat{\Delta p'_L}$ for two band-pass filtered signals of $-uv_{Q2}$ ($\triangleright$), $-uv_{Q4}$ ($\diamond$), $+v$ ($\square$), and $+u$ ($\circ$), at centre frequencies corresponding to $\lambda \approx 0.03$ m, and $\lambda \approx 0.15$ m.

often (Nelson *et al.*, 1995); they can also create larger drag forces, as the exposed area is temporarily increased.

According to the second term on the right hand side of eq. (2) a downward directed flow creates negative lift forces (stabilising). This effect is clearly observed in figure 12, as $\overline{\Delta p'_{\mathrm{L}}(u,v)}$ increases with increasing v. This effect was present for all configurations and protrusions. A slight influence of u on the lift force is present for the higher protrusion (right plot), indicating an influence of the Bernoulli lift [first term on the right hand side of eq. (2)]. The $\overline{\Delta p'_{\mathrm{L}}(u,v)}$ measured was not large; about 5 N/m^2 at maximum. The change of the Bernoulli lift [first term on the right hand side of eq. (2)] is probably most dominant at the upstream edge of the cube, as the streamlines are contracted most there. However, there were no measurements at this location.

6.2 Extremes and PDF

We also want to examine whether the maximal velocities correspond to (highly) increased values of the forces on the cube in our present measurements. First of all we want to know which components of velocity or velocity derivatives (called velocity indicator) can create potentially displacing forces. In sections 3 and 4.5 the indicators were discussed. For the quasi-steady mechanism a low frequency positive v or u fluctuation will indicate an increased lift, and a positive u fluctuation will indicate an increased drag. Q_2 and Q_4-events (somehow related to momentum transport) are often linked to increased sediment transport, so the maxima of $-u'v'$ (per quadrant) are regarded as well. For the forces generated by the TWPs, a high frequency positive v is expected to correspond to increased drag.

The time scale of the fluctuations is of importance, as this indicates the size of the eddies responsible for the extreme forces. Therefore the following procedure is followed. First of all, a band-pass filter is applied to the velocity-indicator signals. The central frequency of the pass-band is chosen to correspond to a certain length scale, λ (obtained from Taylor's hypothesis, using $\lambda \approx 0.8\overline{u(y)}/f$, where f is the frequency and $\overline{u(y)}$ the time averaged velocity at height y). This is done for two λ-s, representing small scale (stone size) and large scale (water depth) eddies. Next we see whether the instants of maximum velocity for a certain length scale coincide with those of extreme values of the pressures on the cube. For every filtered velocity indicator, $\Delta p'_{\mathrm{D}}$ or $\Delta p'_{\mathrm{L}}$ is averaged over all instants at which this indicator (with a certain length scale) has a maximum that exceeds a threshold value (three standard deviations). The conditionally averaged pressure is defined as follows:

$$\widehat{p'_{\mathrm{c,I}}} = \frac{1}{n_{\mathrm{i}}} \sum_{i \in S} \Delta p'_{\mathrm{c}}(i)\,, \text{where}\ \ S = i \,|\, I(i) > 3\sigma_{\mathrm{I}} \wedge I(i) = \max\left[I(i-mi); I(i+mi)\right] \qquad (24)$$

where c is L or D, I is the velocity indicator considered, and i the the sample number. Some results for $\widehat{\Delta p'_{\mathrm{D}}}$ are depicted in figure 13. The measured PDF of $\Delta p'_{\mathrm{D}}$ or $\Delta p'_{\mathrm{L}}$ is plotted for reference. The markers on the bars on top represent $\widehat{\Delta p'_{\mathrm{D}}}$, with the same horizontal scale as

31

the PDF (for the maxima of the velocity indicators, for a given length scale). So, a marker placed to the right of the mean value of $\Delta p'_{\mathrm{D}}$ (vertical line), shows that extreme values of the velocity indicator considered coincide with large $\Delta p'_{\mathrm{D}}$. This implies that this velocity indicator indeed indicates increased, potentially displacing, drag forces.

6.3 Mechanisms

For all but the lowest protrusion low frequency u-maxima correspond to the largest $\widehat{\Delta p'_{\mathrm{D}}}$ (indicated by the circular marker on the lowest bar, bottom right plot on figure 13, which is representative for all high protrusions). Q_4-events coincide with high values of $\Delta p'_{\mathrm{D}}$ as well. Q_4-events have previously been seen to correspond to transport at higher Re_* (Thorne *et al.*, 1989; Nelson *et al.*, 1995). This would mean that the drag force is the force responsible for displacing the stones, as the negative values of $\widehat{\Delta p'_{\mathrm{L}}}$ show that $\Delta p'_{\mathrm{L}}$ is negative during the sweep events. Conversely, Q_2-events cause a decreased $\Delta p'_{\mathrm{D}}$ (see diamond-shaped markers in figure 13), and an increased $\Delta p'_{\mathrm{L}}$. The strongly positively skewed log-normal shape of the PDF resembles the PDF of shear stresses on a smooth bed. This could be expected, as the combined drag forces on the particles form the bed shear stress. As $\widehat{\Delta p'_{\mathrm{D},Q2}}$ and $\widehat{\Delta p'_{\mathrm{D},Q4}}$ are consistently higher and lower than the mean, respectively, it might be concluded that Q_4-events create larger force deviations than Q_2-events, causing this skewed distribution.

For the lowest protrusion we can make a few striking observations. The first is that the correlation function in eq. 16 can be fitted to the measured one with realistic values for velocity and autocorrelation (figure 5, top left). Also $\widehat{\Delta p'_{\mathrm{D},v}}$ is above the mean $\Delta p'_{\mathrm{D}}$ for the small scale $+v$ fluctuations (figure 13, top right plot, top panel). Further the PDF is very symmetrical, unlike for the other protrusions. Finally the ratio of $\Delta p'_{\mathrm{D,rms}}/\Delta p'_{\mathrm{L,rms}}$ is much smaller than for the other protrusions. All these facts are an indication that the forces directly created by the TWPs are dominant for the lowest protrusion (or exposure).

It is interesting to see that for the higher protrusions the small scale extreme values of $+v$ near the cube still correspond to slightly increased $\Delta p'_{\mathrm{D}}$ (figure 13, right bottom plot, top panel, square marker). The shape of the predicted $\rho_{\mathrm{dl,wp}}$ can still be observed for the higher protrusions. It is not zero at $\tau = 0$ anymore, and the amplitude is smaller, so other mechanisms are clearly present as well. The amplitude seems to decrease with increasing protrusion. It might indicate a small influence of the TWPs at larger protrusions as well, decreasing with protrusion.

7 Non-equilibrium flows

Now we will compare the non-equilibrium flows (cases B and S) to the uniform flow (case U). The same (kinds of) graphs as discussed in the previous section will be used.

7.1 Beginning of bed (case B)

The flow at the beginning of the bed was measured at two water depths downstream of the beginning of the roughness elements. It can be regarded as a flow condition with only small scale turbulence, as the roughness, which increases the shear has only affected the small scale, near bed, turbulence. Large scale, full depth turbulence structures need longer to develop (Shvidchenko & Pender, 2001).

In figure 8 the difference between the mean velocity, Reynolds stress and standard deviation of flows U and B can be compared. Near the bed both profiles are similar for both the mean velocity and the standard deviation. Only the near-bed r.m.s. of longitudinal velocity is slightly less for the beginning bed than for the uniform case. The bed shear stress is also equal for both cases (see table 1).

The measured ρ_{dl} (figure 5) shows a behaviour as predicted in eq. (17), only the amplitude is much less than for –for example– the uniform case with the lowest protrusion. The timescale is different as well. It is shorter, indicating a smaller size of the dominant eddies. An increasing protrusion gives the same deterioration of the resemblance to the theoretical correlation function, as seen for the U configuration.

The PDFs of $\Delta p'_{\mathrm{D}}$ (top right plot in figure 14) are less skewed than the figure of the equilibrium flow. This supports the idea that the large scale, low frequency, eddies create the large positive excursions of the drag force during $Q4$-events, and these are not present in this configuration, as they need a longer upstream reach with roughness to develop (Shvidchenko & Pender, 2001). The pressure spectra for the U and B configurations are shown in figure 15. It can be seen here that the low frequency (large scale) pressure fluctuations have not yet developed at the beginning of the bed. Both the $\Delta p'_{\mathrm{D}}$ and $\Delta p'_{\mathrm{L}}$ spectra have a decrease below a value of $f/\overline{\overline{u}}$ of about 10 (m^{-1}). The total variance of the spectrum for case U is roughly 50% higher than for case B.

7.2 Backward-facing step (case S)

A step, with a smooth bed on top, was placed 12 step heights, h_0 ($h_0 = 6$ cm above the stones) upstream of the cube in the flume. The Froude number on the step had to be low to prevent the water surface becoming wavy, so the water depth was increased, and the discharge was decreased (table 1). The cube was placed a few step heights downstream of the (average) re-attachment point, which is located at about 6-8 step heights downstream (Nelson *et al.*, 1995; Xingkui & Fontijn, 1993). In this flow the turbulence structure is changed in the opposite way as that at the beginning of the bed. An increased level of large-scale turbulence is present, originating from the mixing layer between the main flow and the separation bubble behind the step.

The mean flow profiles are depicted in figure 8. The normalised near-bed flow velocity is clearly less than for the U configuration. The Reynolds stress near the bed is approximately the same, and the turbulence intensities of both velocity components are about twice the
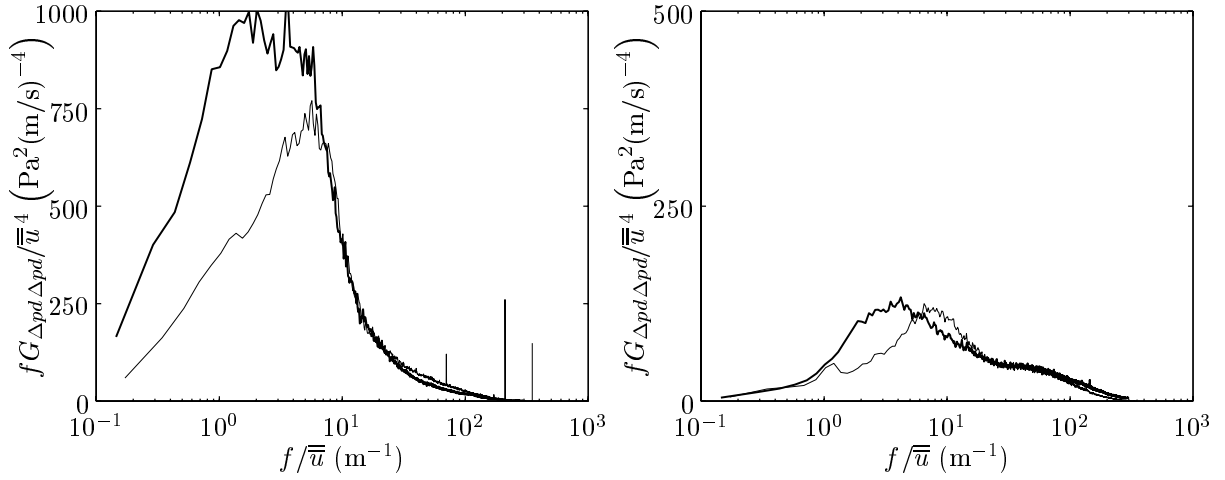
Figure 15: Premultiplied pressure spectra for configurations U (thick line) and B (thin line). left: Δp_{D}, right Δp_{L}. $\Pi = 0$, bed 2.
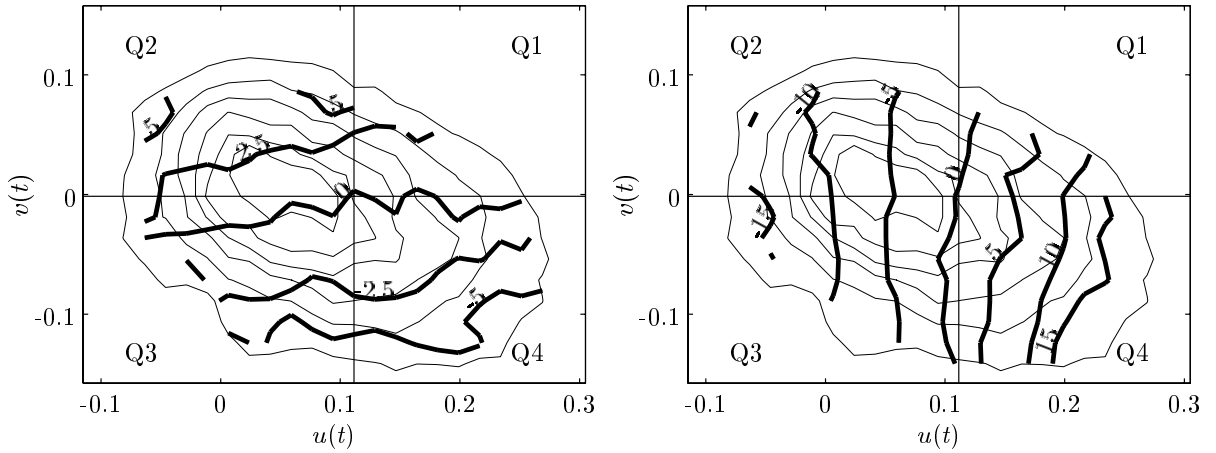

Figure 16: Joint probability density function of $\vec{u}$ (thin isolines), and conditionally averaged pressure (thick isolines) for beginning of bed (B); $\Pi = 1$ cm. Left: $\overline{\Delta p'_{\mathrm{L}}(u, v)}$, right: $\overline{\Delta p'_{\mathrm{D}}(u, v)}$.

34

value for case U. This means that when the bed shear stress ($-\overline{u'v'}$ near bed) is used to indicate the instability of the bed material in the manner of Shields (1936), the ratio of the contributions of the fluctuating forces to the mean forces is not equal, so the dimensionless critical shear stress will be different.

For evaluation of the influence of the TWPs we will now compare the pressures on the top of the cube ($\Delta p'_{\mathrm{L}}$) to measured TWPs near the reattachment point on a smooth wall in a wind tunnel (Lee & Sung, 2002). The pressure sensor on top of the cube for $\Pi = 0$, is placed at the same vertical position as the pressure sensor used in the smooth wall, windtunnel experiments. Only the longitudinal distance is $12\,h_0$ downstream of the step instead of $10\,h_0$ in the windtunnel experiment. It can be expected that the spectra for $12\,h_0$ will be similar to the spectrum at $10\,h_0$, as the spectra for 6, 8, and $10\,h_0$ behind the step were similar as well (Lee & Sung, 2002). The TWPs spectrum for the smooth wall windtunnel experiments overlap the present rough wall measurements for the high frequency range (figure 17, left plot). This implies that the velocity sources for these pressures are situated in the mixing layer, as both the flow near the bed (smooth wall vs. very rough wall), as well as the flow above the mixing layer (developing boundary layer vs. free surface flow), are completely different. It also indicates that these high frequency force fluctuations are directly created by the TWPs. The low-frequency pressures have different characteristics (lower frequency spectral density for the smooth wall increases with f^2, and the present measurements with f^1. Also $G_{\Delta\mathrm{pd}\Delta\mathrm{pd}}$ is very similar to the smooth wall spectrum, resulting in a ratio of $\Delta p'_{\mathrm{D,rms}}/\Delta p'_{\mathrm{L,rms}}$ that is very low (≈ 1).

The isoplots of $\overline{\Delta p_{\mathrm{D}}(u,v)}$ and $\overline{\Delta p_{\mathrm{L}}(u,v)}$ (figure 16) look qualitatively the same as those for case U. Quantitatively, the value of $\overline{\Delta p_{\mathrm{D}}(u,v)}$ (not the fluctuating part, but the total $\overline{\Delta p_{\mathrm{D}}} + \Delta p'_{\mathrm{D}}$) for the same $\vec{u}$ is lower than for case U. Therefore there must be a spatial or frequency dependence which can only be studied with spatial measurements.

The normalised covariance function for case S in figure 5 shows the shape of the theoretical function. The wavelength of the damped sine is longer, indicating a larger size of the dominant eddies. The shape of $\rho_{d,l}$ is shifted downwards, however, giving negative $\rho_{d,l}$ at $\tau = 0$. This indicates that Q_4-events cause simultaneous increased drag and decreased lift.

Although we see from the spectrum that $\Delta p'_{\mathrm{D,rms}}/\Delta p'_{\mathrm{L,rms}} \approx 1$, the extreme value plots (figure 14) tell us something different. The extreme values of Δp_{D} are still caused by increased positive u. $\widehat{\Delta p'_{D,u}}$ is very large compared to $\Delta p'_{\mathrm{D,rms}}$. The occurrence of large positive u excursions is probably less frequently, which results in the very flat PDF for $\Delta p'_{\mathrm{D}}$. The spectrum for $\Pi = 1$ cm is flatter than for $\Pi = 0$. We do see that the high frequency positive v also coincides with an increased drag force, indicating a minor TWP influence.
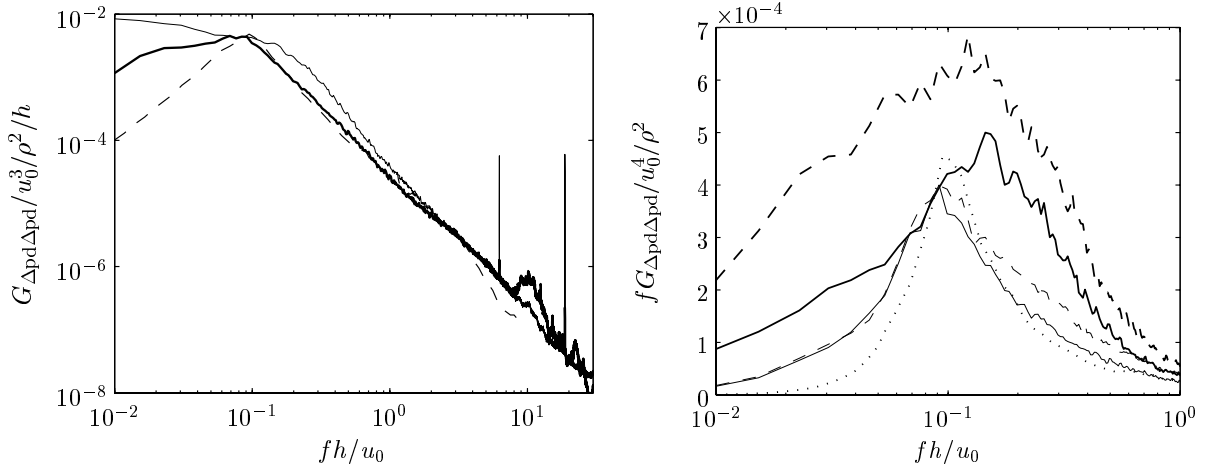
Figure 17: a. (left) Pressure spectra. Dashed line: smooth wall windtunnel WPF behind backward-facing step (Lee & Sung, 2002, $x/h = 10$). Thick solid line: $\Delta p'_L$ (Bed 2, $\Pi = 0$, S). Thin solid line: $\Delta p'_D$ (Bed 2, $\Pi = 0$, S). b. (right) Premultiplied pressure spectra. Dotted line: (Lee & Sung, 2002, $x/h = 10$). Other lines are of the present measurements, bed 2, configuration S. Thin solid line: $\Delta p'_L$, $\Pi = 0$. Thin dashed line: $\Delta p'_D$, $\Pi = 0$. Thick solid line: $\Delta p'_L$, $\Pi = 1$ cm. Thick dashed line: $\Delta p'_D$, $\Pi = 1$ cm.

36

8 Discussion

The effect of protrusion on the character of the forces has been studied in this paper. We saw that the character of the forces changes significantly with changing protrusion. An important question is therefore what the representative value for the protrusion is. This is most likely to be the most protruding particle, as the drag force is larger than the lift force. The protrusion of the most protruding particle available in a just deposited bed will change when flow is applied to this bed. The fact that the most exposed particles are entrained causes a change of the micro bed topography in time. Hofland (2003) used a discrete particle model (DPM) for estimating the particle positions after water-working of the bed. It was concluded from the DPM that particles dropped sequentially at random positions form a surface topography that is highly dependent on the exact properties of the particle-particle collisions. When a simple entrainment model is applied to the beds (removing the most protruding particles) these different beds transform to beds with the same probability distribution of surface characteristics. The "water-worked" bed has a lower protrusion for the most exposed particles. This indicates that there is a universal distribution of particle positions for a (homogeneous) bed under low mobility conditions. On inspection of the PDF of the protrusions, it can be seen that the majority of particles have a relative protrusion under $\Pi/d \approx 0.3$. Therefore the value for the maximum Π in the present measurements ($\Pi/d \approx 0.33$) seems realistic for the most unstable particles in real beds. When the size distribution becomes wider, the protrusions of the large particles will become larger, and that of the small particles will become smaller (Egiazaroff, 1965). This means that for smaller particles the lower protrusions can be typical, which implies that for the smaller particles in a wide gradation, the TWPs-generated pressures can have a significant (dominant) influence on the stability.

If knowledge on the spectrum of forces on a bed particle is to be used for the determination of their entrainment, more effects are of importance. First of all the duration of the forces is of importance. From Newton's second law it follows that the force needed to displace a certain mass (stone) along a certain distance in time T, is proportional to T^{-2} (this is true when the difference between the resisting force and average force is small compared to the amplitude of the fluctuating force). This means that the force needed to displace a stone is proportional to ω^2, which would indicate an influence on the entrainment rate of ω^{-2}. The manner in which a particle will move is of influence as well. The resisting force differs for sliding and rolling particles. Furthermore the wave lengths obtained from a spectrum ($\lambda = 2\pi/k$) are not necessarily equal to the size of an eddy, which can be made up of several components. Therefore the representation with a variance density spectrum does not necessarily give a complete physical description of the fluctuating forces which could dislodge a particle, as can be concluded for the intermittent flow of case S. According to the spectrum the TWPs seem to have a large influence. However, the extreme values of the pressures are corresponding mostly to the quasi-steady mechanism.

An important translation that has to be made is the one from the measured point pres-

sures to forces. It was seen that the horizontal pressure gradient ($\Delta p'_{\mathrm{D}}$) is created by large scale/low frequency flow structures. This means that the pressure point will be representative for the stagnation pressure. Therefore $\Delta p'_{\mathrm{D}}$ and 'drag force fluctuation' are qualitatively interchangeable. For $\Delta p'_{\mathrm{L}}$ this is more difficult. Due to instrumentation reasons the pressure sensor could not be placed at the front of the cube. Therefore the sensor was not present at the leading edge, where streamline contraction, and therefore the largest Bernoulli lift was present. Thus when interchanging $\Delta p'_{\mathrm{L}}$ and lift force, care must be taken, and no direct relation is guaranteed.

9   Conclusions

Only turbulence-generated extreme forces can dislodge particles from a hydraulically rough granular bed under low-mobility conditions. The instantaneous flow field causing these extreme forces on a bed particle is not simply an extension of the mean flow field. It can be seen, for example, that the vertical velocity during extreme excursions of the longitudinal velocity is negative. This can cause a downward stagnation (negative lift) force on the particle during extreme values of the drag force. Therefore it is not realistic to model the extreme forces on a particle simply with an extension of the mechanism that creates the average forces.

The mean horizontal pressure difference $\overline{\Delta p_{\mathrm{D}}}$ was larger than $\overline{\Delta p_{\mathrm{L}}}$. This means that drag is probably the main cause of entrainment, although the angle of repose, the exposed areas, and the distribution of pressure over the surface of the stone still have to be incorporated in the analysis.

From the measurements the following conclusion could be drawn. Drag, caused by longitudinal velocity fluctuations (quasi-steady mechanism), is probably the source for the largest force fluctuations for the most exposed stones. $\Delta p'_{\mathrm{L}}$ was negative during these large values of the drag force, as the large excursions of u coincide with negative v (Q_4-events). The Q_4-events cause the longitudinal velocity to penetrate deeper into the bed and therefore the exposed area of the stone (for the drag force) increases. The negative vertical velocity causes stagnation pressure (negative, stabilising lift) on top of the cube as well. Whether $\Delta p'_{\mathrm{L}}$ is representative for the lift force is not certain. The Bernoulli pressures are probably most intense at the upstream edge of the cube, and were unfortunately not measured.

It has been illustrated that the direct integrated effect of TWPs can lead to forces on granular bed elements. This means that they could be of importance for the entrainment process of granular material. A first situation where this is the case is for stones that are shielded by other stones. In a granular bed that has been water-worked this would be the smaller stones, as they have small protrusions.

The TWPs also have a large influence on the $\Delta p'_{\mathrm{D,rms}}$ and $\Delta p'_{\mathrm{L,rms}}$ when the cube is placed just downstream of the reattachment point of a backward-facing step. The pressures on top of the cube were seen to be mainly determined by the large vortices shed from the step. The

extreme values of the (drag) forces still coincided clearly with an intermittent large increase of u-velocity.

The turbulence above the cube in case B was not completely developed. Especially the large scale fluctuations were not present. Therefore the large scale positive u fluctuations were not present either, making the extreme values of $\Delta p_{\mathrm{D}}'$ much lower. From this it can be concluded that in general bed material is more stable at the beginning of a rough layer, than under developed turbulent flow.

10   Acknowledgements

References

ANDREWS, E.D., & SMITH, J.D. 1992. A Theoretical Model for Calculating Marginal Bedload Transport Rates of Gravel. *In:* BILLI, P., HEY, C.R., THORNE, C.R., & TACCONI, P. (eds), *Dynamics of Gravel-bed Rivers*. New York: John Wiley & Sons.

BLAKE, W.K. 1970. Turbulent boundary-layer wall-pressure fluctuations on smooth and rough walls. *Journal of Fluid Mechanics*, **44**(4), 637–660.

BOOIJ, R. 1998. *Erosion under a geometrically open filter*. Tech. rept. 2-98. Delft University of Technology. In Dutch.

CHENG, NIAN-SHENG, & CHIEW, YEE-MENG. 1998. Pickup probability for sediment entrainment. *Journal of Hydraulic Engineering*, **124**(2), 232–335.

COLEMAN, N.L. 1972. The drag coefficient of a stationary sphere on a boundary of similar spheres. *La Houille Blanche*, 17–21.

CUR. 1995. *Manual on the use of rock in hydraulic engineering*. Tech. rept. 169. RWS, Road and Hydraulic Engineering Division, Gouda.

DOLIGALSKI, T.L., SMITH, C.R., & WALKER, J.D.A. 1994. Vortex interactions with walls. *Annual Review of Fluid Mechanics*, **26**, 573–616.

EGIAZAROFF, I.V. 1965. Calculation of nonuniform sediment concentrations. *Journal of the Hydraulics Division, Proceedings of ASCE.*, **91**(HY4), 225–247.

EINSTEIN, H.A., & EL-SAMNI, E.A. 1949. Hydrodynamic forces on a rough wall. *Reviews of Modern Physics*, **21**(3), 520–524.

FARABEE, T.M., & CASARELLA, M.J. 1991. Spectral featurs of wall pressure fluctuations beneath turbulent boundary layers. *Physics of Fluids A*, **3**(10), 2410–2420.

FENTON, J.D., & ABBOT, J.E. 1977. Initial movement of grains in a stream bed: the effect of relative protrusion. *Proceedings of the Royal Society of London, Series A*, **352**, 523–537.

GEORGE, W.K., BEUTHER, P.D., & ARNDT, R.E.A. 1984. Pressure spectra in turbulent free shear flows. *Journal of Fluid Mechanics*, **148**, 148–191.

GRASS, A.J. 1970. Initial instability of fine bed sands. *Journal of the Hydraulics Division, Proceedings of ASCE.*, **96**(HY3), 619–632.

GRAVANTE, S.P., NAGUIB, A.M., WARK, C.E., & NAGIB, H.M. 1998. Characterization of the pressure fluctuations under a fully developed turbulent boundary layer. *AIAA Journal*, **36**(10).

GYR, A., & SCHMID, A. 1997. Turbulent flows over smooth erodible sand beds in flumes. *Journal of Hydraulic Research*, **35**(4), 525–544.

HOFLAND, B. 2000. *Stability of stones in the top layer of a granular filter – literature survey.* Tech. rept. 07-00. Delft University of Technology.

HOFLAND, B. 2003. Discussion of 'Discrete particle modeling of entrainment from flat, uniformly sized sediment beds' by McEwan, I. and Heald, J. *Journal of Hydraulic Engineering*, **129**(1).

KALINSKE, A.A. 1947. Movement of sediments as bed load in rivers. *Trans. Am. Geophys. Union*, **28**(4), 615–621.

LEE, I., & SUNG, H.J. 2002. Multiple-arrayed pressure measurement for investigation of the unsteady flow structure of a reattaching shear layer. *Journal of Fluid Mechanics*, **463**, 377–402.

NELSON, J.M., SHREVE, R.L., MCLEAN, S.R., & DRAKE, T.G. 1995. Role of near-bed turbulence structure in bed load transport and bed form mechanics. *Water Resources Research*, **31**(8), 2071–2086.

PAINTAL, A.S. 1971. Concept of critical shear stress in loose boundary open channels. *Journal of Hydraulic Research*, **9**(1), 91–113.

PAPANICOLAOU, A.N., DIPLAS, P., EVAGGELOPOULOS, N., & FOTOPOULOS, S. 2002. Stochastic Incipient Motion Criterion for Spheres under Various Packing Conditions. *Journal of Hydraulic Engineering*, **128**(4), 369–379.

PILARCZYK, K.W. 2001 (September). Unification of stability formulae for revetments. *In: Proc. XXIX IAHR congress.*

RADECKE, H. VAN, & SCHULZ-DUBOIS, E.O. 1988 (July). Linear Response of Fluctuating Forces to Turbulent Velocity Components. *In: Applications of Laser Anemometry to Fluid Mechanics.*

RAUPACH, R.M. 1981. Conditional statistics of Reynolds stress in rough-wall and smooth-wall turbulent boundary layers. *Journal of Fluid Mechanics*, **108**, 363–382.

SCHEWE, G. 1983. On the structure and resolution of wall-pressure fluctuations associated with turbulent boundary-layer flow. *Journal of Fluid Mechanics*, **134**, 311–328.

SHIELDS, A. 1936. Anwendung der Aehnlichkeitsmechanik und der Turbulenzforschung auf die Geschiebebetrieb. *Mitteilungen der Preussischen Versuchsanstalt fur Wasserbau und Schiffbau*, **Heft 26**.

SHVIDCHENKO, A.B., & PENDER, G. 2001. Macroturbulent structure of open-channel flow over gravel beds. *Water Resources Research*, **37**(3), 709–719.

SUTHERLAND, A.J. 1967. Proposed Mechanism for Sediment Entrainment by Turbulent Flows. *Journal of Geophysical Research*, **72**(24), 6183–6194.

THORNE, P.D., WILLIAMS, J.J., & HEATHERSHAW, A.D. 1989. In situ measurements of marine gravel threshold and transport. *Sedimentology*, **36**, 61–74.

WATTERS, G.Z., & RAO, M.V.P. 1971. Hydrodynamic effects of seepage on bed particles. *Journal of the Hydraulics Division, Proceedings of ASCE.*, **97**(HY3), 421–439.

WHITE, C.M. 1940. The equilibrium of grains on the bed of a stream. *Proceedings of the Royal Society of London, Series A*, **174**, 322–338.

WIBERG, P.L., & SMITH, D. 1987. Calculations of the critical shear stress for motion of uniform and heterogeneous sediments. *Water Resources Research*, **23**(8), 1471–1480.

XINGKUI, W., & FONTIJN, H.L. 1993. Experimental study of the hydrodynamic forces on a bed element in an open channel with a backward-facing step. *Journal of Fluids and Structures*, **7**, 299–318.

Appendix B. Paper to be published in proceedings for Monte Veritá symposium

ENTRAINMENT OF LARGE PARTICLES FROM GRANULAR BED PROTECTIONS UNDER LOW-MOBILITY TRANSPORT CONDITIONS

BAS HOFLAND, ROB BOOIJ AND HENRI L. FONTIJN
Fluid Mechanics Section, Faculty of Civil Engineering and Geosciences, Delft University of Technology. PO BOX 5048, 2600 GA Delft, The Netherlands. e-mail: B.Hofland@citg.tudelft.nl

1. Introduction: Bed protections and sediment transport

In this paper the stability of bed protections is treated as a special form of sediment transport. The influence of turbulence fluctuations on the stability of bed protections is discussed and examined with the aid of measurements.

Layers of stone are often used to protect the soil around hydraulic structures against scour. The protective layers are constructed in order not to move, although some movement of rocks is allowed. The design value for the Shields factor, $u_*^2/((\rho_s/\rho-1)gd)$, is low, around 0.035 (Pilarczyk, 2001). The stones can be very large (decimeters to meters), giving very high particle Reynolds numbers (typically: $Re_* \equiv u_*d/\nu \approx 10^3$ to 10^5). The rocks are usually obtained directly from a quarry, making the shape very angular, and the size distribution relatively narrow. Furthermore, as the protections have a finite size and are always applied near structures obstructing the flow, non-equilibrium flow and transport are of importance. However, the influence of non-equilibrium turbulence profiles on transport is not clear. This is therefore the main focus of study.

Damage to a bed protection already occurs under low mobility transport conditions (Shields factor under the "critical" value 0.056). In this regime no bed forms are present. Stones move occasionally during extreme events in the flow in the form of sliding and rolling. Only some stones are small, unstable, and/or exposed enough to move. This implies that the flow can be regarded as a flow over a fixed bed, and there will be a limited influence of the moving stones on each other. The characteristics mentioned above (narrow size distribution, flow as over a fixed bed, high Re_*), imply that transport of stones from bed protections can be regarded as a simplified form of sediment transport. It becomes feasible to describe the probability of entrainment by regarding the probability density function (p.d.f.) of the positions of the most exposed stones (varying per stone) and of the forces on the stones (varying in time) as introduced by Grass (1971). The micro bed topography can be regarded as a stochastically distributed boundary value for the strength of a single particle, which may only vary slowly in time, because of repositioning of the top particles.

2. Measurements

Simultaneous pressure and velocity measurements were executed in a 15 m long and 0.5 m wide flume in order to see which turbulence events cause the extreme forces on a particle.

Miniature, low range, piezometric pressure transducers (HONEYWELL) were installed in three sides of a bed-mounted cube (model stone, see Figure 1). The fluctuating pressures could be measured accurately (error < 10 N/m^2, sampling frequency 500 Hz). The cube was part of a one layer thick granular bed consisting of stones with a diameter, d, of about 3 cm. The flow type was open channel flow. A two component laser doppler set-up was used to measure flow velocities. The effect of the protrusion

of the cube, Π, on the character of the fluctuating pressures was investigated by changing Π from 0 to 1 cm. The measurements show that the fluctuating pressures on the cube change significantly when altering Π. The ratios of lift to drag, and of fluctuating pressures to mean pressure are not constant, for instance. Nevertheless, only the cube with $\Pi = 1$ cm ($\approx 0.3d$) is discussed next, as this protrusion is representative for the most unstable particles in a uniformly sized bed. In the following we will focus on the extreme velocity events that cause the maximum forces.

3. Velocity indicators

In order to see which velocity fluctuations induce large forces on a stone, a few mechanisms that possibly generate forces will be discussed, and subsequently linked to the measured pressures on and velocities near the cube.

Indicators for the fluctuating drag and lift forces are obtained from the measured pressures by $\Delta p'_D = p'_1 - p'_3$ and $\Delta p'_L = -p'_2$, respectively (see Figure 1).

The average drag force is mainly caused by the stagnation pressure and the fact that (because of flow separation) the pressure does not build up at the lee side of the stone. The lift force is due to the asymmetric flow over the cube, which causes differences in pressure on either side (Bernoulli's law). Both relations have the form $F = \frac{1}{2}\rho C A u^2$. If u slowly changes, then this "quasi-steady" flow leads to fluctuating lift and drag forces on the stone proportional to $U u' + u'^2$ ($\propto u'$ for $u' \ll U$).

Booij (1998) suggested that the pressure fluctuations that are inherent to a turbulent flow field can also cause net forces on a stone, which might aid in the entrainment of particles. These fluctuating pressures are linked to the inertia of the accelerating and decelerating water parcels above the bed. The horizontal and vertical components of the resulting forces on a stone caused by this mechanism will be addressed as the potential drag and lift force. The adjective "potential" is used, as the velocity-pressure relation is described by potential flow theory, contrary to the quasi-steady drag described before which is caused by viscosity related flow separation at the downstream side of the stone (Lighthill, 1986). In order to see which velocity fluctuations might be linked to these forces we start with the Euler equation (no viscous terms, as Re_* is high):

$$-\frac{1}{\rho}\nabla p = \frac{D\vec{u}}{Dt} \tag{1}$$

and combine this with the buoyancy force on a body in a constant pressure gradient:

$$F_x = -d^3 \frac{\partial p}{\partial x} \tag{2}$$

Subsequently we take: $V=0$, $W=0$, $\partial U/\partial x=0$, $\partial U/\partial z=0$, and $u_i'\partial u'/\partial x_i \ll U\partial u'/\partial x$ (the last simplification is a reasonable assumption, but not generally true). Now we obtain:

$$F_x' \propto v'\frac{\partial U}{\partial y} + \frac{Du'}{Dt} \tag{3}$$

The material derivative of u' in eq. (3) cannot be measured by a one-point measurement, but v' can.

It is also reasonable to assume that, when the momentum transfer towards the bed is large, the resulting forces on the stones are increased. Although the average momentum transfer is equal to $-\overline{u'v'}$, the fluctuating momentum transfer is: $-(uv)' \approx -Uv' - u'v'$, for extreme values of u.

Finally, the presence of certain coherent structures is often linked to the position of the velocity vector on the u',v' plane, which is divided into four quadrants, Q_i. During sweeps (Q_4: $u'>0$, $v'<0$) and ejections (Q_2: $u'<0$, $v'>0$) the value of $-u'v'$ is positive. This means that this term enables us to link the presence of coherent structures to the extreme forces on particles, although only a point measurement is available. This term is not equal to the momentum transfer.

Summarizing, the following velocity indicators can be obtained. Extreme values of u' should correspond to extreme drag and lift forces caused by quasi-steady forces. The largest quasi-steady forces are expected to have a longer duration, as the low frequency u-fluctuations contain more energy. Extreme values of $+v'$ could correspond to the extreme potential drag force, see eq. (3). This force can be expected to have a short duration, as the pressure gradients increase with decreasing eddy size. The fluctuating momentum transfer is given by $-Uv'-u'v'$. The term $-u'v'$ is related to certain coherent structures. The last two indicators describe indirect causes of increased forces on a stone, and the corresponding velocity indicators can therefore be expected to have a correlation to the forces, when measured at higher positions in the flow.

Now we examine whether the maximum values of these indicators correspond to increased values of the forces on the cube in our present measurements. The length scale of the fluctuations is of importance, as this indicates the size of the eddies responsible for the extreme forces. Therefore the following procedure is followed. First of all, a band-pass filter is applied to the velocity-indicator signals. The central frequency of the pass-band is chosen to correspond to a certain length scale, λ, (obtained from Taylor's hypothesis, using $\lambda = 0.8U(y)/f$, where f is the frequency and $U(y)$ the time averaged velocity at height y). This is done for two λ's, representing small scale (stone size) and large scale (water depth) eddies. Next we see whether the instants of maximum velocity for a certain length scale coincide with those of extreme values of the pressures on the cube. For every filtered velocity indicator, $\Delta p'_D$ is averaged over all instants at which this indicator (at a certain height, and with a certain length scale) has a maximum that exceeds a threshold value (three standard deviations). The results for $\Delta p'_D$ are depicted in Figure 2. The measured p.d.f. of $\Delta p'_D$ is plotted for reference. The skewed log-normal shape resembles the p.d.f. of shear stresses on a smooth bed. This could be expected, as the combined drag forces on the particles form the bed shear stress. The markers on the bars on top represent the conditionally averaged values of $\Delta p'_D$ (for the maxima of the velocity indicators, at a certain height and for a given length scale). So, a marker placed to the right of the mean value of $\Delta p'_D$ (vertical line), shows that extreme values of the considered velocity indicator coincide with large $\Delta p'_D$. This implies that this velocity indicator indeed indicates increased, potentially displacing, drag forces.

We can see that low frequency u'-maxima near the cube correspond to the largest $\Delta p'_D$ (indicated by the circular marker on the lowest bar). Further away from the cube ($y = 54$ mm $\approx 1.5d$) the sweeps coincide with the highest values of $\Delta p'_D$. Sweeps have previously been seen to correspond to transport at higher Re_* (Williams et al. 1986; Nelson et al., 1995). This would mean that the drag force is the force responsible for displacing the stones, as the conditional averages of $\Delta p'_L$ show that $\Delta p'_L$ is negative during the sweep events. Conversely, ejections cause a decreased $\Delta p'_D$ (see diamond-shaped markers in Figure 2), and an increased $\Delta p'_L$. It is interesting to see that the

small scale extreme values of $+v'$ near the cube correspond to slightly increased $\Delta p'_D$ (Figure 2, square marker), which might indicate a small influence of the potential forces as well.

4. Conclusions

We consider the protruding cube ($\Pi/d = 0.3$), as it is a realistic model for an unstable stone. The horizontal pressure gradient (both mean and fluctuating) was much larger than the vertical gradient. This means that drag is probably the main cause of entrainment, although the angle of repose and the exposed areas of the stone still have to be incorporated in the analysis. Fluctuating lift might be necessary for the entrainment if the angle of repose is high (smaller particles). Near the cube extreme values of u' coincides with the largest $\Delta p'_D$. At higher elevations in the flow ($y = 54$ mm) sweeps coincide with larger $\Delta p'_D$ than extreme values of u'. It must be mentioned that the type of flow structure leading to a "sweep" (Q_4-event) near a rough bed is not clearly defined at present, contrary to the smooth bed case.

Flow configurations with an altered turbulence structure will be studied as well. A PIV installation is being set up for measurements of entire flow fields.

5. Literature

Booij, R. (1998) *Erosion under a geometrically open filter*. Tech. Report. 2-98, Delft University of Technology. In Dutch.

Grass, A.J. (1971) *Initial instability of fine bed sands*. Journal of the Hydraulics Division, Proc. of ASCE, **96**(HY3), 619–632

HONEYWELL, http://catalog.sensing.honeywell.com/datasheet.asp?PN=24PCEFA6D. Data sheet of pressure sensors, type 24PCEFA6D.

Lighthill, J. (1986). *Fundamentals concerning wave loading on offshore structures*. Journal of Fluid Mechanics **173**. 667–681.

Nelson, J.M. Shreve, R.L. McLean, R. and Drake, T.G. (1995) *Role of near-bed turbulence structure in bed load transport and bed form mechanics*. Water Resources Research **31**(8).

Pilarczyk, K.W. (2001) *Unification of stability formulae for revetments*. Proc. XXIX IAHR Congress, Beijing, theme E.

Williams, J.J. Thorne, P.D. and Heathershaw, A.D. (1986). *Measurements of turbulence in the benthic boundary layer over a gravel bed*. Sedimentology **36**. 959–970.
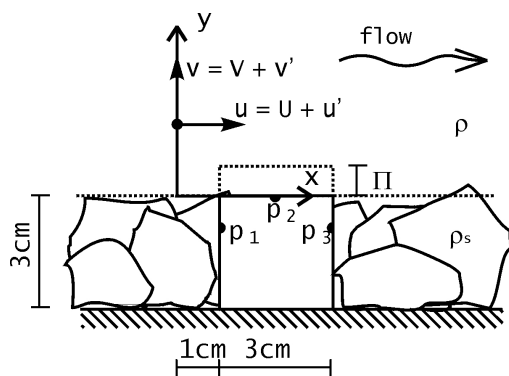
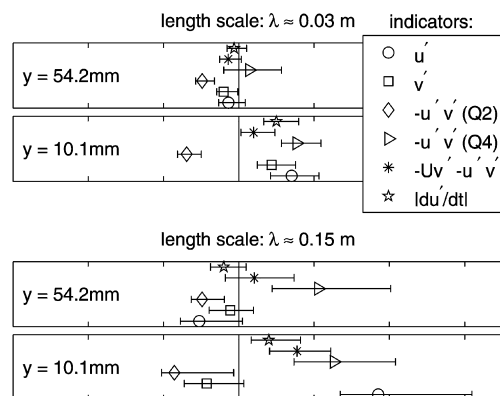Fig 1. (top) Pressure transducers in granular bed with definition of symbols.
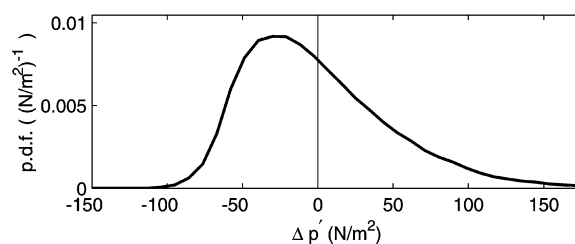
Fig 2. (right) Markers: conditionally averaged $\Delta p'_D$ on the basis of band-pass filtered signals of various velocity indicators (see legend). Below: p.d.f. of $\Delta p'_D$. All horizontal axes have the same scale.

Appendix C. Discussion for Journal of Hydraulic Engineering regarding DPM

Discussion of "Discrete Particle Modeling of Entrainment from Flat Uniformly Distributed Sediment Beds" by Ian McEwan and John Heald

July 2001, Vol. 127, No. 7, pp. 588–597.

Bas Hofland[1]

[1]PhD Student, Faculty of Civil Engineering and Geosciences, Delft Univ. of Technology, E-mail: B.Hofland@citg.tudelft.nl

The discusser would like to give his compliments to the writers of the paper. The use of a discrete particle model (DPM) represents an important step in research on sediment transport and entrainment. It is a useful research tool, especially for low mobility/ coarse-particle bed load, since the transport of the individual particles is obviously dominated to a large extent by the bed structure in this flow regime. For this reason the discusser has recently developed a very similar DPM for evaluating the critical loads for granular beds, which will be used to make a few remarks.

The writers use a bed formed by dropping particles on the bed at random positions. The particles are not removed or redistributed by the flow. The model is therefore used to determine characteristics of a nonwaterworked bed. It is known that this bed is completely different than a waterworked bed, as the writers state themselves. In the following it is argued that the bed must be waterworked, and that the way in which the particles are deposited initially is not very important to the waterworked bed.

The discusser uses a model similar to the writers', except for the following characteristics:
1. The impacts of the particles are calculated by discrete time integration, using a linear spring constant k and a linear damping constant c.
2. No added mass is incorporated in the hydrodynamic forces.
3. A less sophisticated entrainment model is used. However, unlike the model of the writers, this model is used to actively change the bed structure. The particles protruding most are simply removed from the bed. Fenton and Abbot (1977) have shown that the protrusion is very important to the critical force on a particle. The moving particles are not put back on the bed, as information about jumping/rolling lengths is limited and uncertain. This means that the bed level becomes

lower, however this is not relevant when searching for a general bed geometry that can be related to any mean level.

The particles used for the simulations are much larger than the authors' ($d = 0.1$ m), as the discusser's subject of interest is stability of bed protections, which are usually made up of large stones or rocks. The spring constant for the particle–particle collisions was set to 10^5 N/m. The other parameters were the same. Two simulations were executed in which the damping factor for the particle–particle collisions was varied. The first was executed with a damping factor c of 125 N/(m/s), which gave a rebound velocity for a straight collision of 50% of the incoming velocity. For the second simulation c was 500 N/(m/s), giving a negligible rebound velocity.

In Fig. 1(a) the average protrusion distributions of the two simulated beds are plotted. It can be seen that the distribution of protrusions for particles with a negligible rebound velocity [damping factor $c = 500$ N/(m/s)] is wider than the distribution of protrusions for the particles with a rebound velocity of 50% of the incoming velocity [$c = 125$ N/(m/s)]. This is explained by the fact that particles that bounce a few times before they come to rest at their final position have a higher chance of ending up in a depression in the bed, from which they cannot leave. Conversely, a particle that drops dead immediately has a higher probability of coming to rest on top of an elevation of the bed. This means that a higher rebound velocity (lower c) leads to a flatter bed, which is confirmed in Fig. 1(a). This also agrees with the conclusion of the writers that the depositioning process is of importance for the (initial) bed structure. On close inspection of Fig. 4 of that paper, it can be seen that the distributions of critical "shear stresses" for different particle sizes do not collapse exactly either. This might be caused by different depositioning processes of the various particles, caused by their different sizes.

Now we consider the entrainment process. In realistic situations, the most protruding and unstable particles will be moved immediately, even by a flow with low velocity. After that, less protruding particles are removed, and gradually an equilibrium bed forms. In most research on entrainment and transport, flow is applied to the bed for a certain time to let the bed be waterworked, in order to get a good estimate of the critical entrainment. See for instance the very precise experiments by Paintal (1971). This effect is modeled in a simple way in the discusser's discrete particle model (DPM), by just removing the most protruding ex-
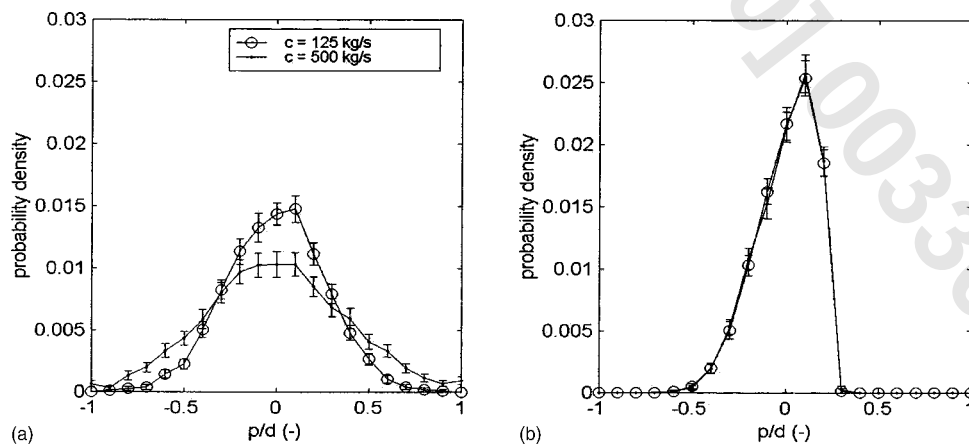

Fig. 1. (a) (left) Initial distribution of protrusions of exposed particles for two simulations with different damping coefficients for particle impacts. (b) (right) Distribution of protrusions of exposed particles for same two beds as (a), after subsequently removing most protruding particles

posed particles. These are the exposed particles positioned at the highest position in the bed. After one particle is removed, the exposed particles are determined again, before the next one is removed, as new exposed particles can be uncovered by removing a particle.

In Fig. 1(b) we can see the distributions of protrusion for both beds, after one (or more) layers of the most protruding exposed particles have been removed. Now the distributions of the two different beds are very similar. This implies that, although the initial geometry of the beds was different, the underlying packing is similar or even equal. This leads to the conclusion that if an entrainment model is used, the method of depositing the particles does not matter much. The geometry will of course depend on the entrainment model.

The above gives the opportunity to evaluate the entrainment model by comparing the bed geometry simulated by the DPM, to a measured bed texture. Measurements can be done as mentioned by Smart (2002). Of course, realistic entrainment processes are more complicated than the simple entrainment model used. However, the fact that the two protrusion distributions overlap after removing the ''most unstable'' particles strongly suggests that the way in which the beds are deposited is not of importance, but rather the way in which the upper particles are removed, or repositioned. Therefore attention should be paid to the kind of entrainment/transport model, instead of the depositioning model of the particles. The presence of large differences of the bed ge-

ometry for the two beds without waterworking means that a model for waterworking must be applied to the bed prior to any statistical analysis of critical forces of the various particles in the bed. This holds especially when it is used to compare the modelling results to empirical results such as the Shields curve or a transport formula.

Notation

The following symbols are used in this paper:

c = damping coefficient;
d = particle diameter;
k = spring constant; and
p = protrusion.

References

Fenton, J. D., and Abbot, J. E. (1977). ''Initial movement of grains in a stream bed: the effect of relative protrusion.'' *Proc. R. Soc. London, Ser. A,* 352, 523–537.

Paintal, A. S. (1971). ''Concept of critical shear stress in loose boundary open channels.'' *J. Hydraul. Res.,* 9(1), 91–108.

Smart, G. M. (2002). ''Relatively rough flow resistance equations.'' *J. Hydraul. Eng.,* 128(6), 568–578.

Appendix D. Description of new experimental set-up

Description of the PIV set-up for investigating the effect of turbulence on the stability of stones in the top layer of a granular filter

Bas Hofland, November 2002

1. Introduction

A description of the main experimental set-up that is being used for the second series of experiments in the PhD project 'stability of stones in the top layer of a granular filter' is presented in this text. The main part of the set-up is the particle-image-velocimetry (PIV) system. It is used to determine the influence of turbulence on stone stability. For this we want to measure the conditionally averaged flow field above a stone during its first movement. One moving stone (target stone) will be considered, while the rest of the bed is immobile. The flow field above the target stone and the pressure field under this flow field will be measured, together with the movement of the stone. Several flow configurations will be investigated. An equilibrium (uniform) open channel flow, the flow at the beginning of a bed (roughness transition) and the flow behind a backward-facing step. These flow types were previously investigated using the laser Doppler technique. This note will mainly describe the PIV set-up and the set up around the target stone.
Most techniques described in this note are already available in the laboratory. At the moment they are still being combined and optimized.

2. PIV general technique

The most common PIV method used these days is double frame / single exposure digital PIV. For the two-dimensional implementation of this technique two separate images are made of an area in a flow. The flow is visualised by adding seeding particles to it. The seeding consists of small particles that refract the light and follow the flow. When one calculates the two-dimensional correlation of small parts (windows) of two sequentially recorded images, the maximum correlation is found at the mean displacement of the seeding particles in the flow. This is a direct indication of the velocity at that 'point'. The images are most often directly made by a CCD camera, therefore all information is digitised from the start. This enables the user to process large amounts of data. A typical camera has 500^2 to 2000^2 pixels, which can be used to obtain a flow field with about 1000 to 60000 vectors. An example plot of two consecutive 32 by 32 pixels windows, and the correlation peak indicating the mean displacement are shown below.
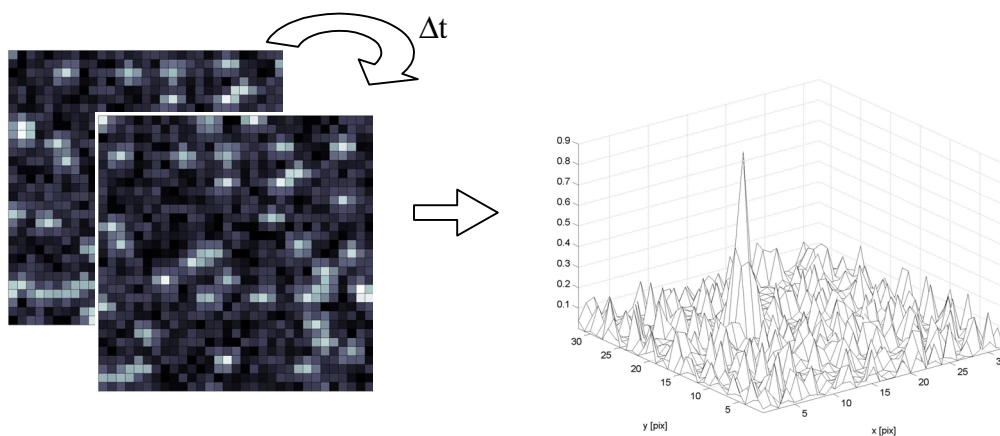

Figure 1. Two (synthetic) 32 by 32 pixels windows, and the resulting peak of the correlation function indicating the displacement.

Most often the seeding particles are very small, therefore a powerful illumination of the measuring area is needed. A laser is often used for this. The coherent light can be shaped to a light sheet, which illuminates the required plane in the flow.

3. Dimensions

The dimensions of the set-up are determined by a number of demands that arise from the requirements posed by the topic of research and practical considerations. The demands are:

Requirement	Norm	Value in set-up
Non-mobile bed	$\tau / \rho \Delta g d \ll 0.04$	0.01
Low-mobility of target stone	$\tau / \rho \Delta_t g d \approx 0.04$	0.044
Fully rough bed	$Re_* > 500$	1200
"Two dimensional" flow	$B / h > 3$	3.3
Uniform flow with logarithmic part	$h / d > 5$	7.5
Narrow grading	$d_{85}/d_{15} < 1.5$	?
Stone large enough for pressure sensors	$d > 1.5$ cm	2 cm

In the table above the required value of the most important design parameters are given. The right column gives values that can be obtained in the experimental set-up, if we assume: mean velocity $\overline{u} = 0.5$ m/s, stone diameter $d = 0.02$ m, water depth $h = 0.15$ m, dimensionless specific density of target stone, $\Delta_t = 0.4$ ($\rho_s = 1400$ N/m^3). It can be seen in the table that the requirements can be met with the measurement set-up These values are indicative for the uniform flow. When the turbulence structure is changed, the critical Shields parameter ($[\tau / \rho \Delta g d]_{critical}$) changes. However, we want the micro bed structure to remain intact, while the target stone still remains in a critical situation. Therefore the density of the fake stone will be changed.

The low mobility of the stones implies that there are no bed forms, and that the stones stay in contact with the bed when they move, so they will be sliding or rolling. We will try to have a rolling stone, as that is convenient for the measurements (the stone can be fixed with a hinge). If this is not possible (this will follow from trial measurements), another method will have to be found.

4. Flume

A 25m long by 0.5 m wide flume was constructed with had a few special characteristics. First it has a closed-loop water system, as it is not possible to seed the whole water supply of the laboratory. Second, the inflow and outflow are isolated from the flume (only connection is a 2 mm rubber slab) in order to minimize the vibrations of the flume, which can interfere with the pressure measurements. Further a slope was constructed in the outflow, which is intended to decrease the waves in the flume. The inflow is smooth and converging, making the flow as quiet as possible.

5. PIV system used

A dedicated system from LaVision will be used to measure streamwise 2DV velocity fields. The method that is used is double frame / single exposure (two separate images are made, both of which are illuminated once.) The Kodak ES1.0 camera is especially suited for this method, as the CCD-chip (1000 by 1000 pixels) is designed for recording two consecutive images with a short time-interval. A 50 mJ double-pulsed Nd:YAG laser is used to illuminate the area of interest. It is especially designed for the method as well. It consists of two pulsed lasers. Special optics in front of the laserset make the two beams overlap. Each laser can have a pulse- frequency of up to 15 Hz. The time interval between the two pulses, however, can be set to very short intervals, up to nanoseconds. In this way a velocity field can be obtained from a wide range of flows, as the interval time between two recorded images can be in a wide range (from 10^{-8} to 10^{2} s).
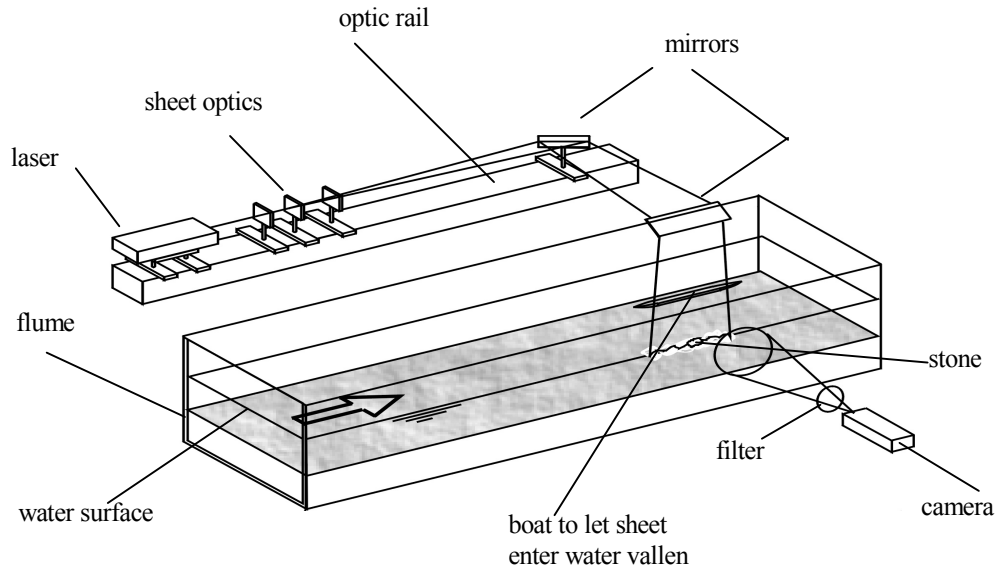
Figure 2. The set-up in the laboratory

In Figure 2 the set-up of the PIV system as constructed in the laboratory is depicted. The distance between optics and measuring area is increased in order keep the divergence angle of the sheet width limited (giving a constant energy over the height). This distance could become very impractical in the limited space available, therefore the optical rail, on which the optics are mounted, is placed in line with the flume, and the laser sheet is guided towards the measuring area using two mirrors. All lenses and mirrors are coated, so that the loss of light is limited.

The sheet optics consist of three lenses. The first after the laser is a spherical lens. The distance from this lens to the measuring area determines the width of the sheet. A positive and a negative cylindrical lens are placed behind just the spherical lens. These lenses determine the thickness of the sheet. Probably a thick sheet is needed, as the turbulence intensity is high, and the out-of-plane motion of seeding particles will be large, creating of loss of correlation between the two images that are used to determine the flow velocity.

A window was made to let the sheet go undisturbed through the water surface. Coated non-reflecting glass is glued on the bottom of a 1 cm wide 'boat' which is streamlined. This 'boat' can be positioned a few mm into the water using micro-positioners.

6. Stones

Fake 'stones' will be made from two-component epoxy resin. This material is easy to cut, so pressure sensors can be placed in them easily (see section 8). These instrumented stones will have to be fixed to the bed, as the material is lighter; otherwise they might move easily. The low specific density of the material makes it very suited for creating the target stone, as the target stone has to move under flows under which the rest of the bed is still immobile. By adding different additives to the epoxy resin (PVC or steel filings), the same stone can be reproduced in a large range of densities. The moulds for making the stones are made from latex (the kind available in art shops).

As the sheet is illuminated from above, the stones on the bed are illuminated by the laser. An intense reflection of the light on the (moving) stone could damage the camera. In order to avoid this, the stones could be shielded by placing something between the stone and the camera. However, in this case the velocity near the stone cannot be measured. So we would like to include the stone image directly in our image. The movement of the stone can then be determined from the image as well. For this the following method is used. The stones under the sheet are painted with fluorescent (Rhodamine-based) paint, and a green-bandpass filter is placed in front of the camera lens. In this way the green light reflected from the seeding reaches the CCD and (a large part of) the reflected light from the stones becomes red, and is

stopped by the optical filter. From trial tests we saw that with the optical filter in place, the amount of light from the laser could become 4 times larger than without the filter. This makes the difference between a successful and an unsuccessful measurement.

If the stones are placed on a straight floor, the porosity near the bed is higher. In order to keep the porosity near the bed at the value of the porosity in the stone bed, the first layer of stones will be put in a layer of cement, making the porosity at the interface between the granular layer and the impermeable bed (almost) equal to the value inside the stone bed.

7. Triggering

2 GB of memory is available in the PC of the PIV system. This means that around 30 seconds of 15 Hz frames can be stored in RAM. Measurements have to be stored in RAM, as the scusi-drive is not fast enough to write double images with 15 Hz to disk.

The way in which we will record the flow events during the initiation of motion needed to make the conditional averages will be described next. There is a possibility to record images in a ring buffer, which means that every new image replaces the oldest image in memory. This is depicted in the next figure. During measurements we wait for a stone to move; when this happens, the program we will wait for a fixed period, 10 s for example, and after these 10 s the data measured from 10 s before until 10 s after the event can be written to disk. Now we wait until the stone falls back into place. When it moves again, and the same procedure is repeated. This whole process can be automated, if we have an automatic trigger signal, indicating the stone movement. This signal is created by placing a piece of metal-foil on the moving stone at the place of the contact point with the upstream stone, and placing an inductive sensor in the stone under the contact point. As soon as the stone moves, the ring buffer is triggered. This system is schematically depicted in Figure 3.
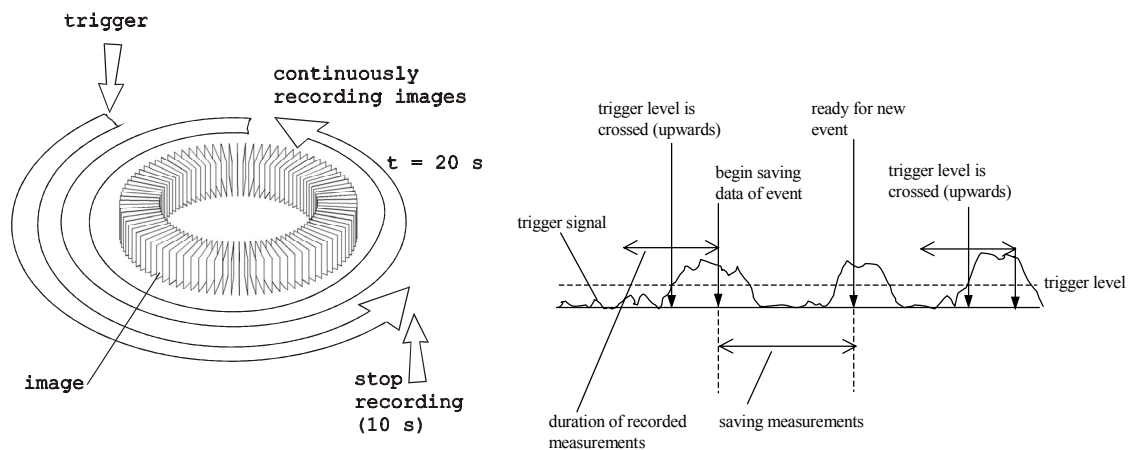
Figure 3.   Schematic representation of ring buffer (left) and trigger signal including typical order of events (right).

The program DaVis, which is used for the data-acquisition, has the possibilities of receiving an external trigger signal and of using a ring buffer already. With the macro language that is part of the system it should be possible to combine this into the described system.

8. Set-up around stones

Pressure sensors will be placed around the stone in order to measure the pressure field simultaneously to the velocity field. They are of the same type as used in the first measurement series. There is only place for one sensor per stone, so the direction will have to be chosen. As usually the fluctuating lift forces have small length scales, the spatial coherence will be limited, therefore we will put sensors pointing upwards in

line with the velocity field. The drag force usually has larger length scales, so sensors pointing horizontally upstream can be placed next to the centerline (where the velocities are measured), while the relation between velocity and drag force can still be examined. One sensor is placed in the stone below the target stone, as it is unknown what happens to the pressure under the stone at the moment it moves. The target stone is fixed with a hinge, keeping it at a fixed position and orientation during all measurements. The way in which the target stone, all pressure sensors around it, the hinge, and the inductive motion sensor are placed together is depicted in Figure 4.
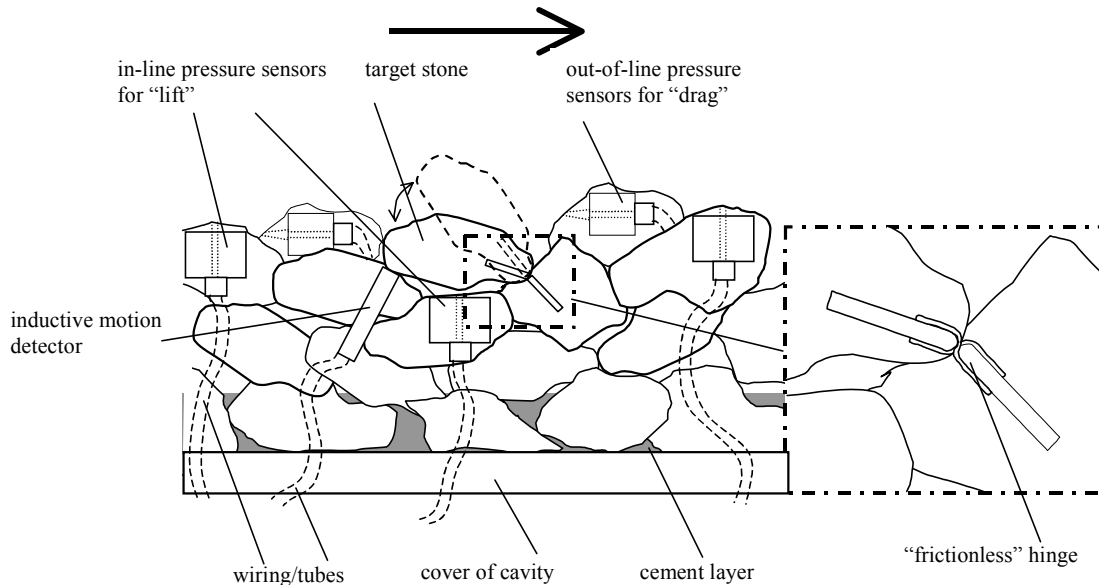
Figure 4. Set-up around the target stone

9. Seeding

In order to 'see' the flow, seeding particles have to be added to the flow. There must be enough particles in the flow so that per window we have at least 10-15 particles. A particle taking up at least 2 pixels is best, as its position can then be determined with sub-pixel accuracy, as the correlation peak will consist of more than one point with various gray values, through which a line can be fitted. This would mean that particles of around 150 μm should be used. Hollow glass spheres of 10 μm are available. They are very suited as seeding particles. They are (almost) neutrally buoyant, and the air inside also reflects the light very well. However, they are too small to fill several pixels. This can be changed by slightly defocusing the camera, thereby increasing the particle image size. This method was tried, and seemed to work. An advantage of using small particles is that they are less likely to accumulate in the pores of the granular bed, which could pose a problem, as the flow would lose its seeding very quickly.

Figure 5. Measured percentage of good vectors, as a function of seeding concentration.

Appendix E. Laser safety report

Veiligheidsrapport
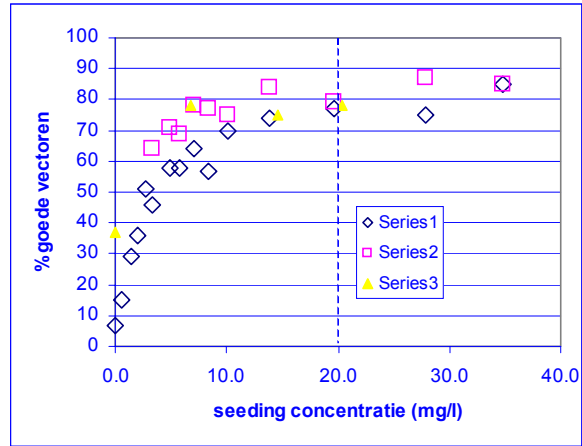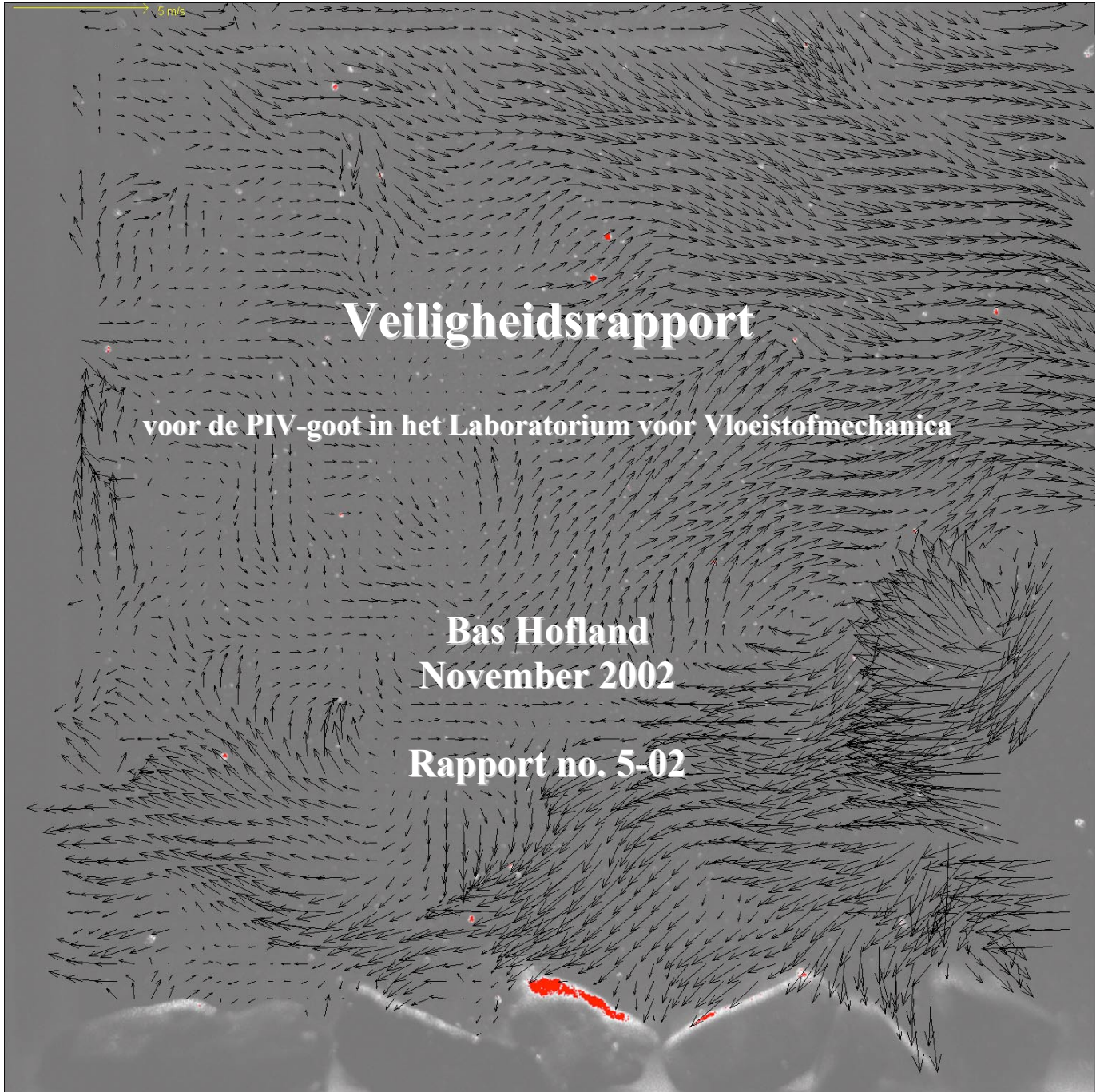
voor de PIV-goot in het Laboratorium voor Vloeistofmechanica

Bas Hofland
November 2002

Rapport no. 5-02

Delft Cluster

TUDelft

1. Inleiding

Voor de experimenten die in het kader van het promotieonderzoek "Stabiliteit van grofkorrelige structuren" uitgevoerd worden is het gewenst om instantaan stromingsvelden te kunnen meten. Hiervoor kan de zgn. PIV (particle-image velocimetry) techniek worden gebruikt. De digitale versie van deze techniek is de laatste jaren een geschikt en populair middel geworden om instantane snelheidsvelden te meten. De krachtige Nd: YAG laser (veiligheidsklasse 4) die gebruikt wordt voor de hier besproken implementatie kan schadelijk zijn voor het oog of de huid. In dit rapport worden de veiligheidsmaatregelen die daarom genomen moeten worden bij de metingen vastgelegd. De metingen zullen eind 2002 beginnen en tot mei 2003 duren.

1.1. Aandachtspunten

De veiligheidssituatie bij deze experimenten wordt gecompliceerd door het feit dat:
- het Laboratorium voor Vloeistofmechanica vrij toegankelijk is;
- de metingen nabij spiegelende wateroppervlakken en ruiten gebeuren;
- de gehele stroom van (doorzichtig) water moeilijk geheel af te sluiten is door de grote lengte van de goot (25 m).

Een positief punt is dat:
- bij de PIV techniek de straal divergent gemaakt wordt, zodat hij minder schadelijk is dan bij bijv. een laser-doppler techniek, waar de straal convergent wordt gemaakt.

1.2. Inhoud van rapport

Voor dit rapport is als voorbeeld het TU rapport (sectie Vloeistofmechanica, faculteit Civiele Techniek), no. 15-94 gebruikt. Dit rapport was weer gebaseerd op het IAVM rapport no. 12 'Richtlijnen laserveiligheid, voor research en onderwijs' (1986). In hoofdstuk twee worden beschreven: de gebruikte apparatuur, de opstelling en de veiligheidsmaatregelen die genomen (moeten) worden. In de bijlagen staan o.a. plattegronden, een accoordverklaring van de laserwerkers en extra informatie over de apparatuur.

2. Veiligheid Apparatuur en Opstelling

2.1. PIV

Bij de gebruikte Particle Image Velocimetry (PIV) techniek worden met een kleine tussentijd twee opnamen gemaakt van een doorsnede in het water. Dit water is "vervuild" met kleine seedingdeeltjes om de beweging zichtbaar te maken. Door kleine gebiedjes uit de twee opnames te correleren zijn de richting en grootte van de snelheid van het water in dat betreffende gebiedje te bepalen. Alle snelheden samen resulteren in een meting van het instantane snelheidsveld over het opnamegebied. Om de kleine deeltjes goed te kunnen visualiseren, moeten ze belicht worden door een sterke lichtbron. De Nd:YAG lasers zijn hier ideaal voor omdat ze heel korte pulsen geven. Door twee parallelle lasers te gebruiken is het tijdsinterval tussen de twee opnamen (die benodigd zijn voor een schatting van een snelheidsveld) te variëren tot elke gewenste waarde.

2.2. Beschrijving opstelling

De Nd:YAG laserset bestaat uit twee lasers die pulsen laserlicht uitzenden met een hoge intensiteit. Door optiek direct achter de lasers (bevindt zich nog in de laser-module) worden de laserstralen over elkaar heen gelegd, en komen ze door dezelfde opening naar buiten. Deze laserstralen hebben een maximale energie van 50 mJ en een maximale frequentie van 15 Hz. De sturing en voeding van de laser is compact en klein. Hierin bevindt zich ook de waterkoeling. De laserstralen worden gebruikt om een vlak te verlichten. Hiertoe wordt de straal (in één richting) opgeblazen, waardoor de straal overal divergerend is. Dit maakt de opstelling veiliger dan bij de laser-doppler techniek, waar de stralen juist geconvergeerd worden.

Het doel van de metingen is het bepalen van het snelheidsveld boven een stenenbodem. Hiertoe wordt het lichtvlak van bovenaf door het wateroppervlak naar beneden geschenen. Het laserlicht raakt de stenen op de bodem van de stroomgoot en wordt vervolgens gereflecteerd. De stenen zijn met fluorescerend-rode verf (op rhodamine basis) beschilderd om reflecties tijdens het meten uit de opname te kunnen filteren. Er wordt dus rood en groen licht weerkaatst vanaf de stenen. De stroomgoot waarin de laser wordt toegepast is ca. 25 m lang en 0.5 m breed. Een plattegrond is getekend in bijlage A. Omdat de goot in een nauwe ruimte tussen drie andere goten staat (de carrousel, de 2-meter goot, en de oude golfgoot) is er maar vanaf één kant toegang tot de meetplaats.

2.3. Laag vermogen

Het vermogen van de laser kan in twee trappen worden ingesteld. Ten eerste op de voeding van de laser (*High* / *Low*). Daarnaast door de timing van de zgn. *Q-switch*. Deze timing bepaalt het moment dat de fotonen uit de laserbuis worden gelaten. Omdat de hoeveelheid fotonen varieert in de tijd, kan zo de energie per puls worden geregeld. De timing van de laser wordt geregeld via het softwarepakket DaVis. Hieronder staan de gemeten vermogens van de twee lasers.
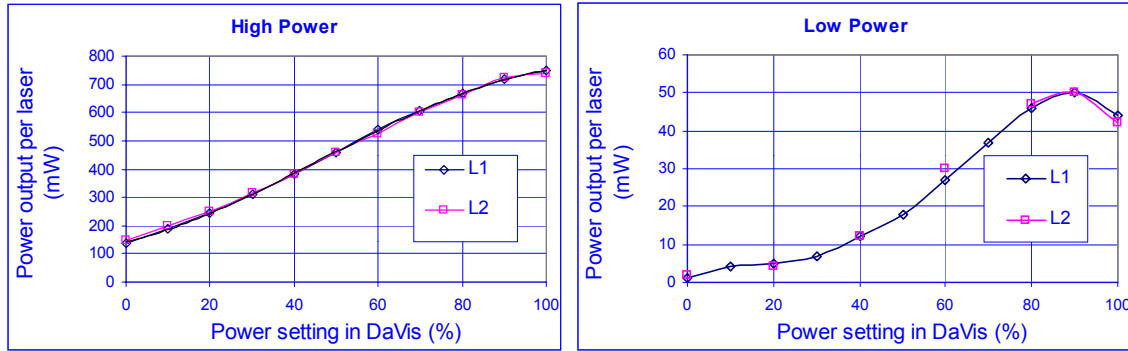
Figuur 1: Gemeten output van de laser, per laser. Power setting in het programma DaVis, en setting op de laser (high/low).

Het uitlijnen van de laser kan veilig kan bij een instelling van *Low* op de laser en 0 in DaVis. Hierbij mag uiteraard nog steeds niet direct in de straal gekeken worden!

2.4. Optisch pad

De laseropstelling staat hieronder schematisch getekend. De laserstraal gaat door drie lenzen. Hierna volgt een lang pad waarlangs het vlak langzaam divergeert in breedterichting. Vervolgens wordt d.m.v. twee spiegels het pad omgebogen en valt het licht van boven, door het wateroppervlak, in het water. Door het wateroppervlak steekt een gestroomlijnd glazen plaatje ("bootje"). Dit heeft als doel om het wateroppervlak geen verstorend effect op de stralengang te laten hebben. In bijlage B staan de diverse afstanden tussen lenzen, spiegels, etc vermeld.
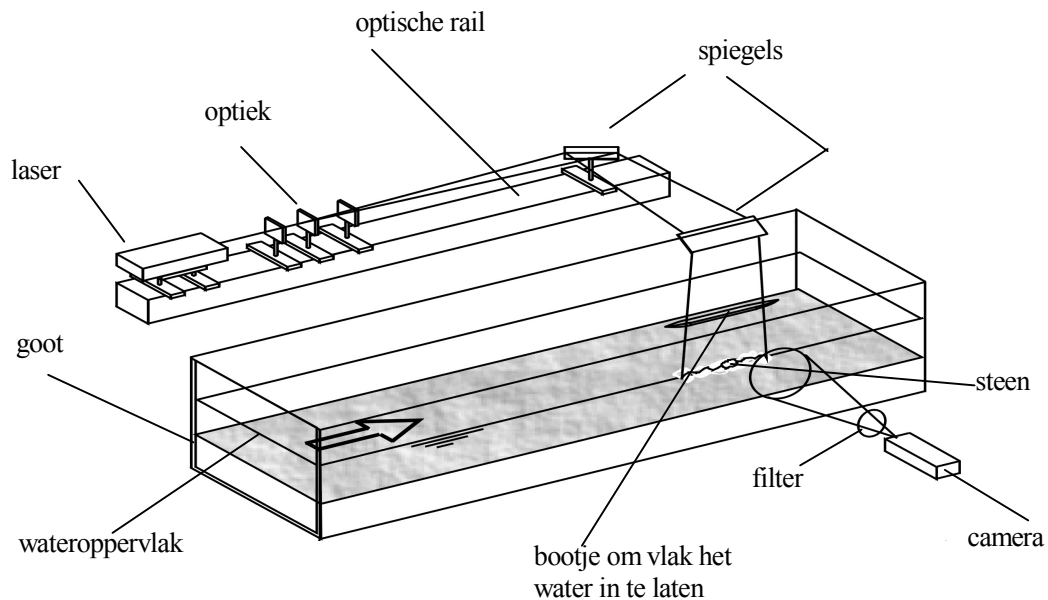
Figuur 2: Schematische tekening van de laseropstelling

2.5. Vermogen van de stralen.

Als de straal de laser verlaat is het vermogen 1.5 W (gemiddeld over de pulsen en de twee lasers). Dat geeft in het midden van de straal (diameter=3.5 mm) een vermogensdichtheid van $\approx 7*10^5$ W/m^2. Hierna divergeert de bundel en in het meetvlak is de vermogensdichtheid nog maar $\approx 7*10^3$ W/m^2.

Omdat de pulsen redelijk frequent gegeven worden, beschouwen we ze als een continue straal. Voor een evenwijdige straal is een vuistregel dat de vermogensdichtheid lager moet zijn dan 1μW/cm^2. Dit is gelijk aan 10^{-2} W/m^2 (gebaseerd op een maximaal toelaatbare energie op het netvlies van 0.1 J/cm^2, een veiligheidsfactor 0.1, een concentratiefactor 10^6 en een belichtingstijd van 0.1 sec). Het laservlak is divergent, dus de mogelijke schade zal minder erg zijn, dan deze berekening doet vermoeden. De straal zal wel tot en met de tweede reflectie afgeschermd moeten worden.

2.6. Afscherming

2.6.1. Optisch pad

Het hele optische pad van laser tot en met meetvlak (straal heeft zeer hoge intensiteit) wordt afgesloten tijdens het gebruik van de laser. De afscherming staat getekend op bijlage C, in rode lijnen. Het is een kist om de optische rail heen. Verder volgt de kist het pad van de laserstraal. Op de bovenkant zitten twee deksels die open kunnen scharnieren.

2.6.2. Goot

De goot bestaat uit elementen van 1.5 m lengte en heeft glazen wanden en een open bovenkant. De bovenkant en de zijkanten kunnen gemakkelijk afgeschermd worden met houten platen. Hier komt maximaal een eerste, diffuse reflectie op. De afscherming moet ergens ophouden, omdat de gehele goot te lang is om helemaal af te schermen. Er is voor gekozen om de afscherming naast en op de goot over twee en een half element aan weerszijden van de meetsectie door te laten lopen (3.75 m). In de goot zelf komt boven het wateroppervlak een zware zwarte doek te hangen, zodat de reflecties in de langsrichting van de goot grotendeels worden afgeschermd (vooral de omhooggerichte, die het grootste gevaar vormen om iemands oog te treffen). Er blijft nu altijd een gat in de afscherming, daar het water zelf niet afgesloten kan worden en het doorzichtig is. Het gat is echter zover weg dat weinig licht tot hier toe zal doordringen. Ook is het lichtvlak divergent, zodat de intensiteit sterk is afgenomen. Verder is de hoek van een eventueel naar buiten komende straal zo flauw, dat hij totaal zal reflecteren en binnen de goot zal blijven, of –in geval van een reflectie op het wateroppervlak– op de bodem zal komen, waarna er na de tweede diffuse reflectie weinig lichtsterkte overblijft.

2.6.3. Veiligheidsschakelaar

De deksels op de kist om de optische rail zijn verbonden met schakelaars, die verhinderen dat de laserset aan kan als een van de deksels open is, en de laserset direct uitzetten als de deksels tijdens het meten worden geopend. Ook zijn de schakelaar verbonden met een rode noodknop op de voorzijde van de kist, waarmee de laserset ook uitgeschakeld kan worden.

Voor het uitlijnen is het soms nodig om de laser toch aan te hebben (op minimaal vermogen) bij geopende deksels. Er is hiertoe een (beveiligde) schakelaar aangebracht. Als deze wordt omgezet is dit mogelijk. Wel treedt er dan tegelijkertijd een waarschuwingsgeluid / -lichtsignaal in werking, wat de laserwerker er continu aan herinnert dat de situatie gevaarlijk kan zijn. Ook slaat de laser na een aantal (zo'n 5) minuten alsnog vanzelf af.

2.6.4. Toegang

De enige toegang tot het meetgedeelte bevindt zich in de ruimte tussen de PIV-goot en de 2 meter goot. Deze is makkelijk af te schermen door een lint en een waarschuwingsbord.

2.6.5. Aanduiding onveiligheid

De potentiële onveiligheid van de opstelling wordt voor onbevoegden duidelijk gemaakt, door aan alle kanten stickers te plakken waarop gewaarschuwd wordt voor de laserstraling.

2.7.   Procedure

Voordat de laserwerker met de opstelling en de laser mag werken dient hij/zij dit rapport gelezen te hebben, waaronder de punten beschreven in bijlagen D en H, en dit ook verklaard te hebben d.m.v. het tekenen van bijlage G. Dit alles in samenspraak met de lokale laserdeskundige.

Bijlagen

A. Plattegrond opstelling
B. Optiek
C. Tekening van de afschermingen
D. Werkvoorschrift
E. Lijst laserwerkers
F. Specificaties laser en opstelling
G. Accoordverklaring laserwerkers
H. Te nemen veiligheidsmaatregelen bij het werken met lasers

A. Plattegrond opstelling

Maten in cm.

B. Optiek

Zijaanzicht

sp. 1 sp. 2

90 mm 95 mm 1700 mm 150 mm

3.5 mm

ca. 2 mm

-30 mm +60 mm -25.4 mm

Boven - aanzicht

150 mm

3.5 mm

-30 mm 0 mm 0 mm
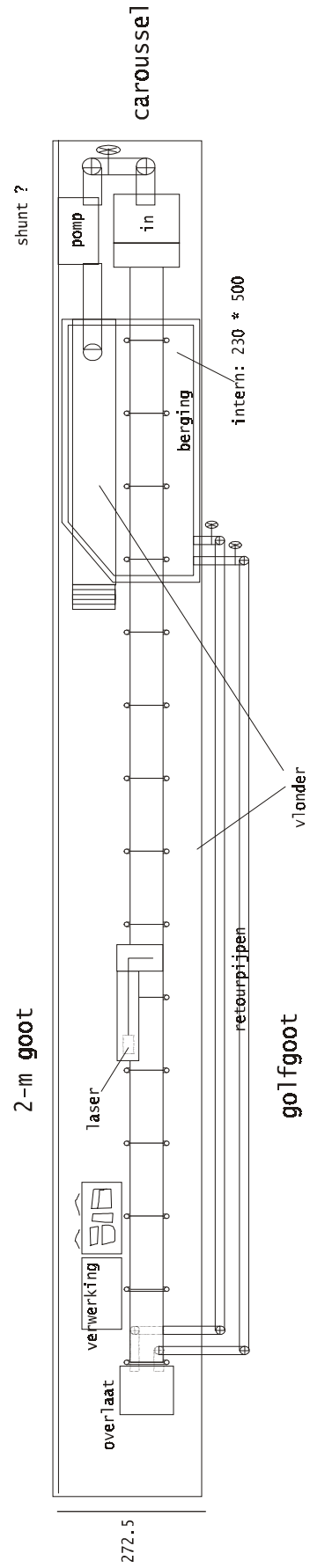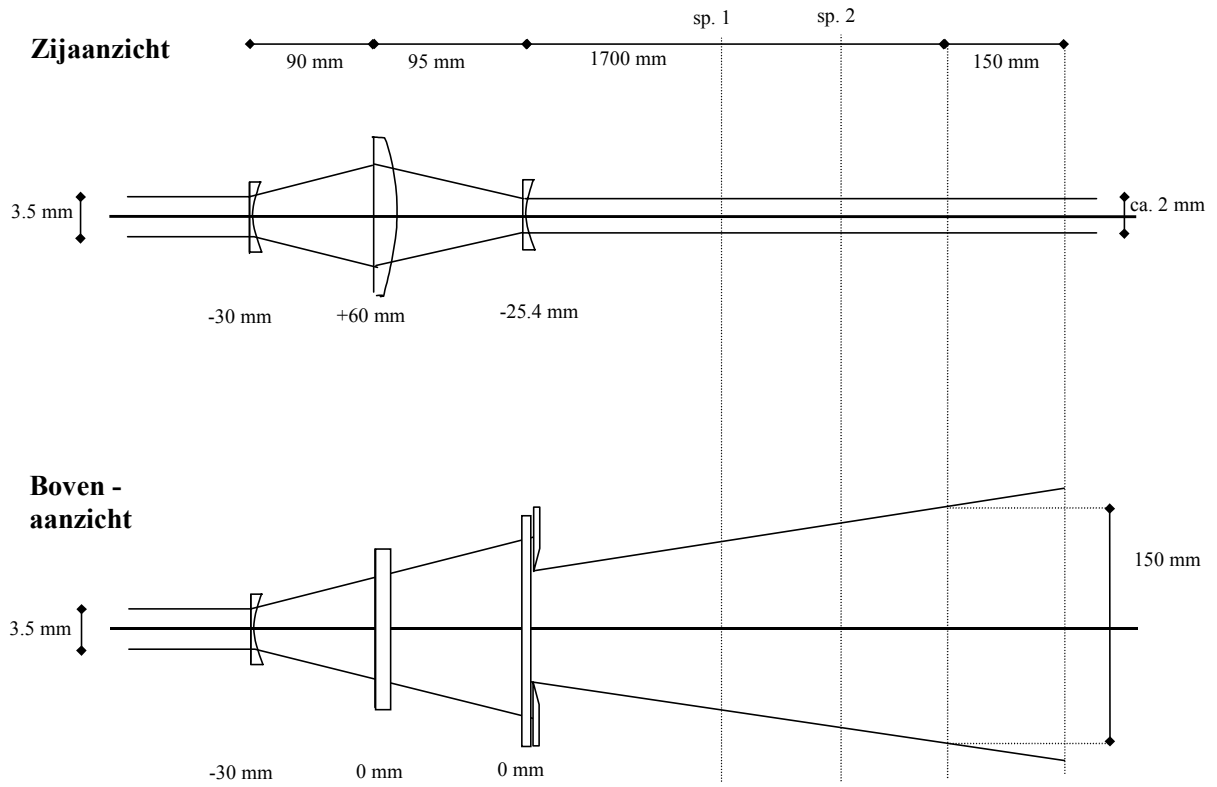
Optiek-configuratie voor het maken van het lichtvlak.

C. Tekening van de afschermingen

blauw: afscherming goot
rood: directe afscherming laserpad, van binnen bekleed met brandwerend materiaal

Veiligheidskist voor PIV-goot
20-8-2002
Bas

maten in mm

maat door balk bepaald

410

500

400

700

binnenkant (rode gedeelte) met brandwerende stof bekleed

afneembaar
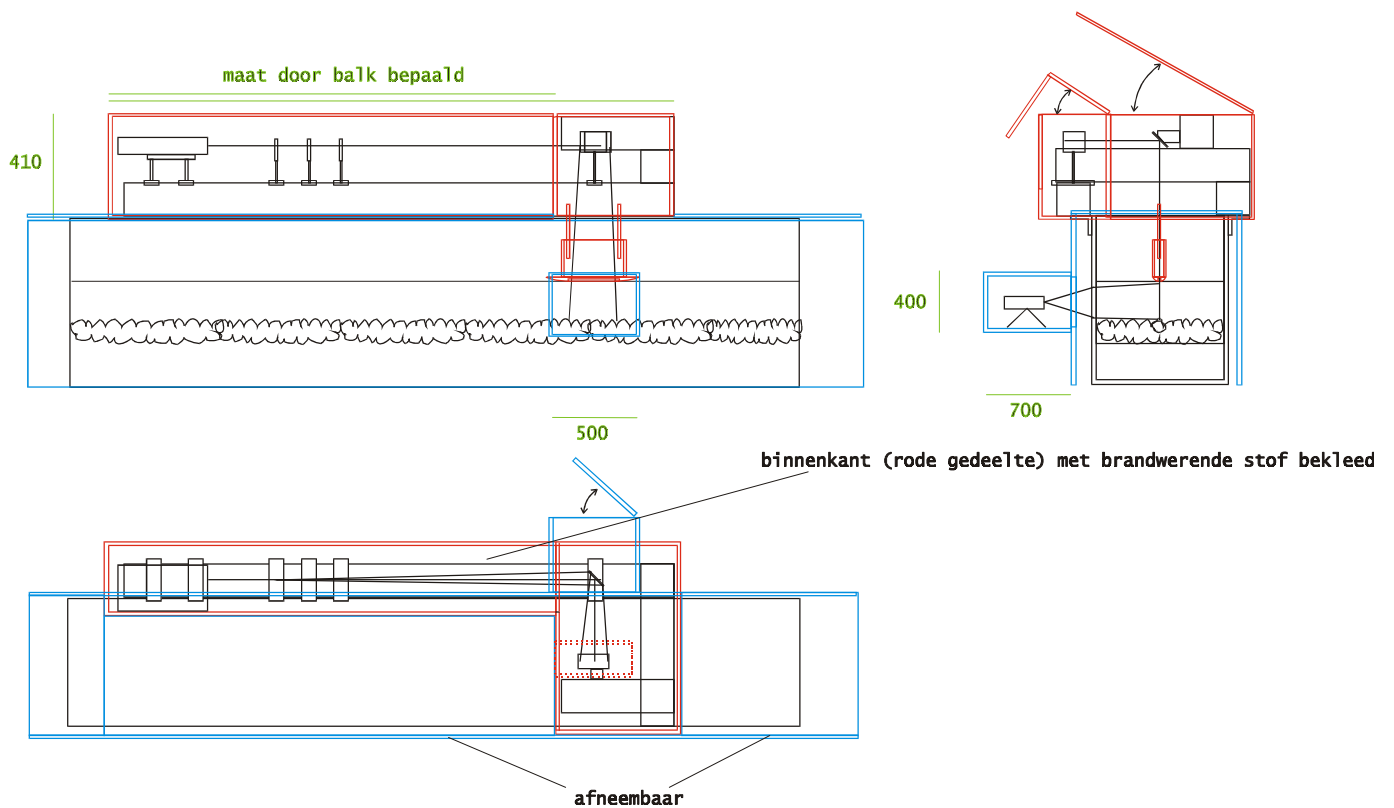
D. Werkvoorschrift

De afstelling van het lichtvlak vindt in de volgende fases plaats:
- eerst wordt de loop van de straal nagegaan zonder laserlicht (staan alle lenzen e.d. ongeveer goed?);
- daarna worden eventuele reflecties opgespoord bij **minimaal vermogen** (zie bijlage H);
- hierna kunnen de breedte en dikte van het vlak ingesteld worden bij minimaal vermogen;
- tenslotte worden de deksels gesloten en de beveiliging aangezet.

Als de laserwerker **tests** wil doen met **hoger vermogen**, zoals het meten van het straalprofiel, het bepalen van de overlap van de twee stralen, etc. dan dient:
- de laser naar de (afgeschermde) laserkamer verplaatst te worden.
- hier wordt dan een beschermende laserbril gedragen.

Voordat met proeven met **hoger vermogen** wordt begonnen:
- wordt gecontroleerd of de stroming in evenwicht is, zodat het wateroppervlak niet gaat dalen;
- wordt het looppad versperd voor onbevoegden;
- worden de deksels dichtgedaan en vergrendeld;
- wordt de electronische beveiliging aangezet;
- wordt de afscherming van de goot aangebracht en vastgeschroefd;
- wordt de afscherming van de goot gecontroleerd.

Zie verder "te nemen veiligheidsmaatregelen bij het werken met lasers" (bijlage H)

Afwijkingen van de werkvoorschriften vereisen overleg met en toestemming van de lokale laserdeskundige!!

E. Lijst Laserwerkers

Oktober 2002

Algemene gegevens

Faculteit: Civiele Techniek en Geowetenschappen
Afdeling: Waterbouwkunde en Geotechniek
Sectie: Vloestofmechanica
Gebouw: Laboratorium voor Vloeistofmechanica, gebouw Stevin III
Beheerder: dr ir H.L. Fontijn

Toegelaten laserwerkers

ing. M. v.d. Meer	coördinator instrumentatie
ir B. Hofland	promovendus
dr ir W.S.J. Uijttewaal	lokale laserdeskundige / senior onderzoeker
drs R. Booij	senior onderzoeker
R. de Ruiter	afstudeerder

F. Specificaties Laser en opstelling

Algemeen

Faculteit:	Civiele Techniek en Geowetenschappen
Afdeling:	Waterbouwkunde en Geotechniek
Sectie:	Vloestofmechanica
Gebouw:	Laboratorium voor vloeistofmechanica, Stevin III

Beheerder: dr ir H.L. Fontijn
Lokale laserdeskundige: dr ir W.S.J. Uittewaal

Project: Stabiliteit van granulaire bodembeschermingen
Projectleider: ir B. Hofland

Laser

Klasse:	4
Soort laser:	dubbele, gepulste, YAG-laser
Laser medium:	Nd: YAG
Golflengten:	532 nm en 1064 nm
Bundeldiameter ($1/e^2$):	3.5 mm
Wordt doorsnede kleiner:	neen
Max. energie per puls per laser:	50 mJ
Frequentie:	15 Hz
Pulsduur:	3-5 ns
Max. gem. vermogen:	1.5 W (2 lasers * 15 Hz * 50 mJ)
Max. gem.vermogensdichtheid (gem. over pulsen en beide lasers)	
Hoofdbundel	$\approx 7*10^5$ W/m^2
Meetvlak	$\approx 7*10^3$ W/m^2
Aard van bundel:	divergent
Spanning:	220 V

Fabrikant laser:	New Wave
Model/type:	Solo PIV III
Registratienummer	16094
Leverancier:	LaVision

Karakter werkruimte:	Open hal
Opstelling:	Optische balk op de goot met direct er omheen een afscherming
Toegang:	Tussen twee goten loopt het pad dat naar de meetplaats voert.
Verdere afscherming:	Zij- en bovenkant van de goot zijn afgedekt; tijdens metingen wordt looppad met waarschuwingsbord afgezet.

G. Accoordverklaring laserwerkers

In te vullen door lasermederwerker:

Naam: ....

Geboortedatum: ....

Geboorteplaats: ....

Functie: ....

Werkadres: ....

Telefoon werk: ....

Thuisadres: ....

Telefoon thuis: ....

De laserwerker verklaart:

- Een exemplaar van 'Veiligheidsrapport voor PIV-goot in het Laboratorium voor Vloeistofmechanica' te hebben ontvangen en gelezen.

- De voorschriften hierin te zullen naleven

- Het voorschriftenblad 'te nemen veiligheidsmaatregelen bij het werken met lasers' te hebben gelezen.

- Deze voorschriften ook te zullen volgen.

- Door de lokale laserdeskundige te zijn gewezen op de risico's die verbonden zijn aan het werken met lasers.

Plaats: Datum:

         ....

Handtekening laserwerker:

                  ....

Handtekening lokale laserdeskundige:

                  ....

H. Te nemen veiligheidsmaatregelen bij het werken met lasers

Regels.
1. Het pad van de laserstralen moet volledig afgeschermd zijn als er met meer dan minimaal vermogen (timing op 0 (nul) en laser op 'low') wordt gewerkt.
2. Alleen na instructie door en toestemming van de lokale laserdeskundige wordt het iemand toegestaan werkzaamheden met de laser te verrichten.
3. Laserwerkers zijn zij die als zodanig zijn toegelaten.

Laserwerkers dienen:
1. Instructies en voorschriften na te leven.
2. Incidenten te melden aan de lokale laserdeskundige.
3. Ongevallen direct te melden aan de EHBO.

Voorschriften voor de laserwerkers
1. Nooit in de laserstraal kijken.
2. Vermijd huidcontact met laserlicht.
3. Draag geen glimmende artikelen (sieraden, horloges).
4. Verhinder de toegang tot de opstelling (versper looppad naar opstelling).
Bij werken met niet-minimaal vermogen:
5. Doe de directe afscherming dicht, oftewel er moet geen zicht zijn op het pad van de laserstraal van laser tot en met meetvlak.
6. De eerste (spherische negatieve) lens zo min mogelijk verwijderen.
7. Laat genoeg waarschuwingstekens zien.
8. Uitlijnen gebeurt alleen met minimaal vermogen, gedefinieerd als volgt:
    - Stand op laser: low.
    - Stand in DaVis: 0,
        met de volgende instelling in DaVis:

Qswitch delay	Laser 1	Laser 2
max	188	184 μs
min	400	382 μs

Appendix F:
General Appendix, Delft Cluster Research Programme Information

General Appendix: Delft Cluster Research Programme Information

This publication is a result of the Delft Cluster research-program 1999-2002 (ICES-KIS-II),
that consists of 7 research themes:
►Soil and structures, ►Risks due to flooding, ►Coast and river , ►Urban infrastructure, ►Subsurface
management, ►Integrated water resources management, ►Knowledge management.

This publication is part of:

Research Theme	:	Coast and river	
Baseproject name	:	Behaviour of coarse-grained structures	
Project name	:	A: Bed Protections	
Project leader / Institute		dr ir M.R.A. van Gent	WL | Delft Hydraulics
Project number	:	03.02.04	
Project duration	:	01-04-2000 - 31-12-2002	
Financial sponsor(s)	:	Road and Hydraulic Engineering Division of the Ministry of Transport, Public Works and Water Management (DWW)	
		Delft Cluster	
Project participants	:	Delft University of Technology	
Total Project-budget	:	order of magnitude: € 500.000	
Number of involved PhD-students	:	1	
Number of involved PostDocs	:	0	

Delft Cluster is an open knowledge network of five
Delft-based institutes for long-term fundamental strategic
research focussed on the sustainable development of densely
populated delta areas.

Keverling Buismanweg 4
Postbus 69
2600 AB Delft
The Netherlands

Tel: +31-15-269 37 93
Fax: +31-15-269 37 99
info@delftcluster.nl
www.delftcluster.nl

December 2002   Stability of Coarse Granular Structures

Theme leader Coast and River:
prof.dr.ir. M.J.F. Stive (TUD)   M.J.F.Stive@ct.tudelft.nl
 (was: prof. dr ir H.J. De Vriend (WL, TUD, DC))

Project leader DC:
dr ir M.R.A. Van Gent (WL, DC)   Marcel.vanGent@wldelft.nl

Klankbordgroep:
ir G.J. Akkerman (Haskoning, was Ligteringen)   gja@haskoning.nl
ir M.B. De Groot (Geodelft)   m.b.degroot@geodelft.nl
ir J.P.F.M. Janssen (Bouwdienst RWS – WIS)   J.P.F.M.Janssen@bwd.rws.minvenw.nl
ir G. Smith (or Van Gent)   …

Begeleidingsgroep:
prof. dr ir J.A. Battjes (TUD, envisaged promotor)   J.Battjes@ct.tudelft.nl
prof. ir K. d'Angremond (TUD, envisaged promotor)   K.dAngremond@citg.tudelft.nl
dr ir H.L. Fontijn (TUD, daily guidance and project leader TUD) h.l.fontijn@citg.tudelft.nl
drs R. Booij (TUD)   R.Booij@citg.tudelft.nl
ir H.J. Verhagen (TUD)   H.J.Verhagen@citg.tudelft.nl
ir M. v.d. Wal (DWW RWS)   M.vdWal@dww.rws.minvenw.nl
ir H.Verheij (WL|Delft Hydraulics, was dr ir R.Uittenbogaard)   Henk.Verheij@wldelft.nl

Promovendus:
ir B.Hofland   B.Hofland@citg.tudleft.nl